Title

Probing the way of combining theoretical calculation with experimental characterization on deposited single-walled carbon nanotube film

Author

TAN, SHULIN

Publication Date

2019

Peer reviewed|Thesis/dissertation

UNIVERSITY OF CALIFORNIA

Los Angeles

Probing the way of combining theoretical calculation with experimental characterization on deposited single-walled carbon nanotube film

A thesis submitted in partial satisfaction

of the requirement for the degree Master of Science

in Materials Science and Engineering

by

Shulin Tan

2019

ABSTRACT OF THE THESIS

Probing the way of combining theoretical calculation with experimental characterization on deposited single-walled carbon nanotube film

by

Shulin Tan

Master of Science in Materials Science and Engineering

University of California, Los Angeles, 2018

Professor Dwight Streit, Chair

The carbon nanotube has long been seen as a next-generation semiconductor due to its 1D nanostructure and superior electrical properties. However, the characterization of it remains a challenge due to its ultra small diameter. It is suggested that a combination of theoretical simulations and experimental characterization would be suitable to reduce the time and effort needed to probe the properties of the defect of it. In this thesis, both finite element simulation and multiple characterization techniques, namely Raman Spectroscopy, Raman Imaging, Scanning Electron Microscopy and Atomic Force Microscopy, are performed to probe the effect of misalignment on the properties of deposited carbon nanotubes.

The result of finite element simulation shows that the misalignment of nanotubes would lead to a drop in the total current flow through the device and a concentration of electrical current on a

single nanotube. Experiments are then set up to probe a way of characterizing this defect. The diameter and bandgap of the carbon nanotube obtained from characterization is also used in the simulation. It is revealed that computer simulation and characterization results could be combined.

The thesis of Shulin Tan is approved.

Mark S. Goorsky

Jamie Marian

Dwight Christopher Streit, Chair

University of California, Los Angeles

2019

List of figures

List of tables

Acknowledgement

I would like to express my deepest gratitude to my graduate advisor, Professor Dwight Streit, who gave me great support, trust and freedom in doing research in this area. He taught me a lot about how to do research independently. It is a great experience to have him as my graduate advisor. Thank you, Professor Streit.

I would like to express my gratitude to Dr. Haoping Li from ATOM Inc as well, who gave me a lot of support on sample providing and suggestions on characterization setup. He is very experienced in the field of carbon nanotube and I learnt a lot from him.

I also want to express my thanks to Professor Sergey Prikhodko, who helped me a lot in SEM imaging and Raman Spectroscopy.

At the same time, I would like to express my thanks to Dr. Adam Stieg at CNSI, who gave me a lot of support on setting up AFM experiments and hands-on guide on AFM operation.

I would also like to express my thanks to Dr. Naihao Chiang from Professor Paul. Weiss's lab, who helped me set up experiments for Raman Imaging.

I would like to thank Professor Jamie Marian and Professor Mark Goorsky for serving on my thesis committee.

Finally, I would like to thank my family for their selfless support and love.

Table of Contents

1. Introduction

1.1 Motivation

Since its discovery in 1991,[1], carbon nanotube (CNT) has caught the eye of extensive researchers. Not only does it demonstrate superior mechanical properties, such as high strength,[2][3]it also shows potential as a good semiconductor.[4]−[6] Early studies show that carbon nanotubes have high field transmission, high charge carrier mobility and long mean free path of charge carrier. Therefore, it is estimated that its performance could surpass traditional semiconductor materials like silicon.

However, early studies are mostly done on one single carbon nanotube, rather than aligned carbon nanotubes. It remains to be seen how well aligned carbon nanotubes behave and how defects on them will affect its properties. Since carbon nanotube is a 1D material, the defect of the aligned carbon nanotube array would be different from that of traditional semiconductors, which are usually 3D crystalline materials. The characterization of the defects in aligned carbon nanotube as a semiconductor material remains to be a challenge.

There are two main obstacles in characterizing single walled carbon nanotubes arrays. The first obstacle lies in that carbon nanotubes are extremely small in diameter. SWCNT usually have a diameter of 0.4-2nm, which approaches the limit of traditional imaging methods like SEM and AFM. Though TEM has a higher resolution, it requires special sampling methods and may cause some damage to the CNT. The second obstacle lies in that CNTs may be damaged during characterization. It has already been observed that CNTs can be damaged by oxidation,[7]and it is observed in my experiment that long time exposure of electron beam or laser would cause the destruction of CNT. For further characterization, damage should be avoided.

1.2 Objective

The goal of this research is to probe a way of combining computer simulation with experimental characterization of the deposited carbon nanotube. Basic electronic properties, such as material type (semiconducting or metallic), and other basic electrical properties (namely diameter, bandgap and electrical properties) are measured. At the same time, the characterization of the alignment of carbon nanotube is also discussed.

2. Background

2.1 Structure of carbon nanotube

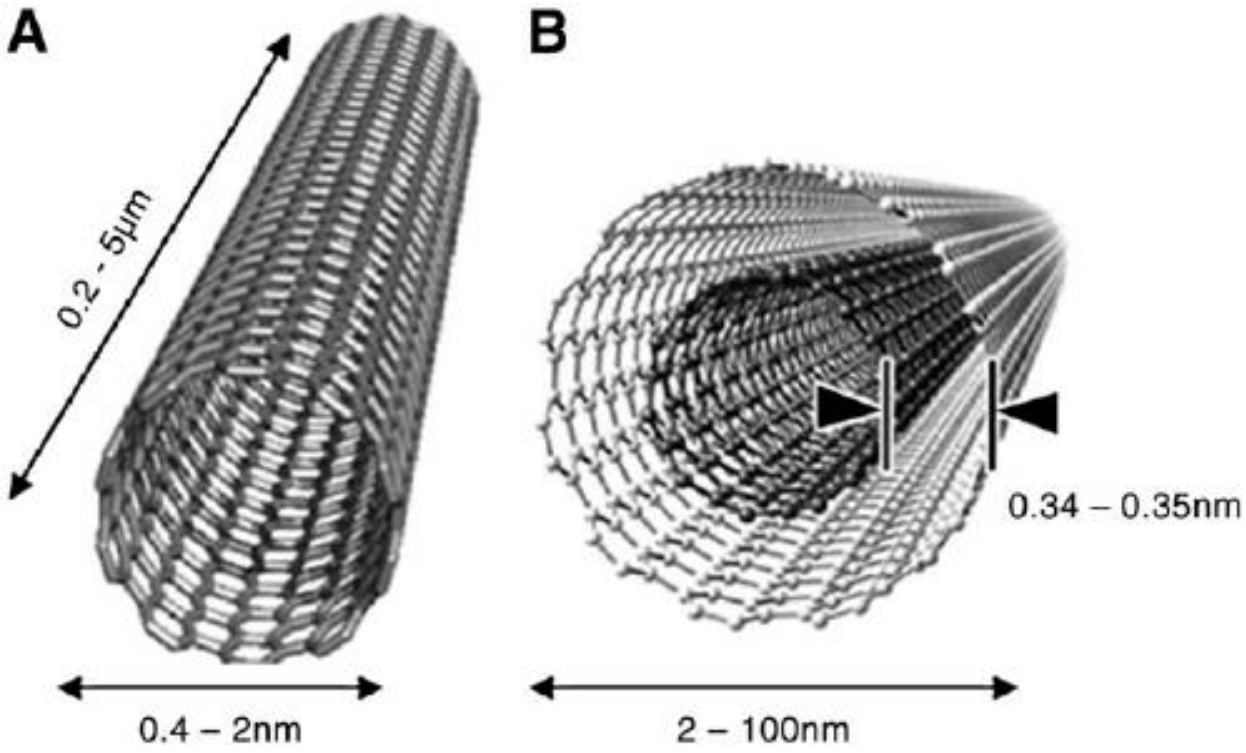

(Fig 2.1: Structure of Single-walled carbon nanotube and Multi-walled carbon nanotube)[8]

Carbon nanotube (CNT) can be seen as graphene rolled up together as a tube.[9] Based on the number of layers of atoms the tube has, CNTs can be divided into single walled carbon nanotubes (SWCNTs) and multi-walled carbon nanotubes (MWCNTs), and their structure is shown in Fig 2.1. MWCNTs typically show no gate modulation since only the outermost layer of carbon is involved in its electron transportation,[6] which makes them not suitable for being fabricated into field-effect transistors. In this thesis, only the characterization of SWCNTs will be discussed.

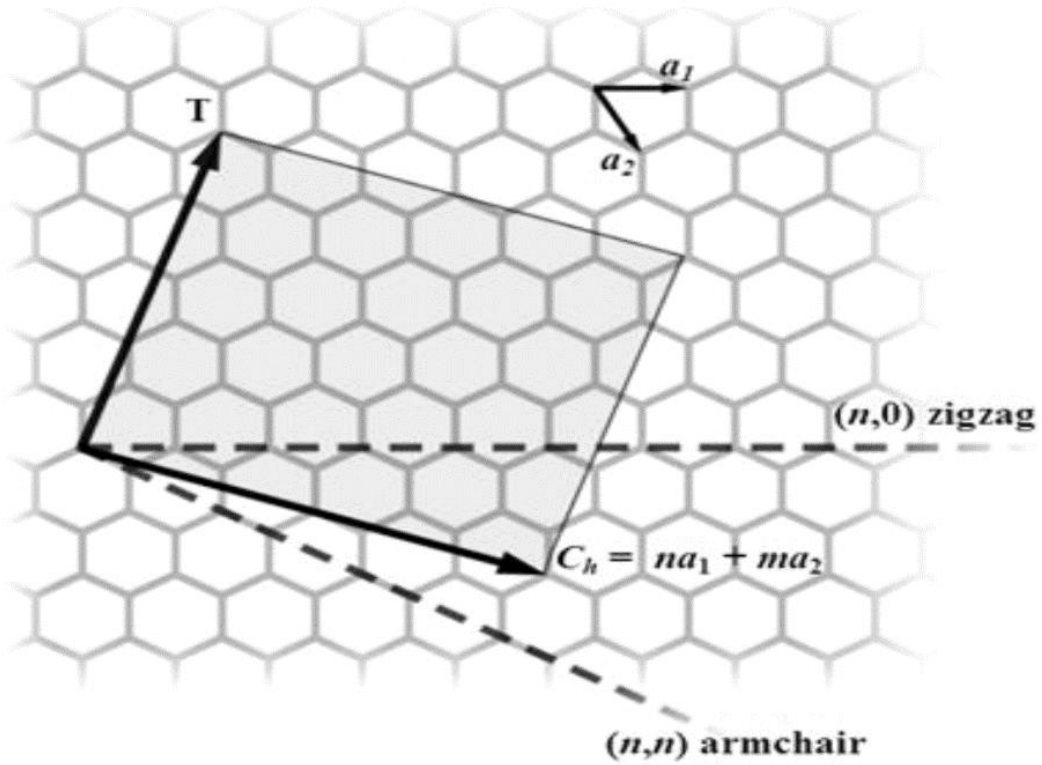

(Fig 2.2: Chirality of single walled carbon nanotube)[10]

The electronic properties of SWCNT is determined by its chirality. Since single walled carbon nanotubes can be seen as a layer of graphene rolled up as a tube, the chirality of it is often described by the vector that denotes the length and direction of the rolling up, $C_h = \mathrm{n}a_1 + ma_2$. a_1 and a_2 are chiral vectors, and n and m are the number of the chiral vectors involved to form C_h, and is usually written as (n,m). This is illustrated in Fig 2.2. A SWCNT is not necessarily semiconducting. If 2n+m=3q (q is an integer), the carbon nanotube is metallic, otherwise it is semiconducting. Therefore, only two thirds of the SWCNTs are semiconducting. Since a metallic carbon nanotube may cause shortcut of the circuit, it is very important to separate the metallic carbon nanotubes and semiconducting carbon nanotubes apart.

The chirality of CNT also determines the diameter of it and thus determines its bandgap.[9]The diameter of a single-walled carbon nanotube is $\sqrt{3}a_{c-c}(m^2 + mn + n^2)^{0.5}$, where

a_{c-c} is the C-C bond length.[11] By measuring the diameter and electrical properties of a carbon nanotube, the chirality of it can be easily measured.[12]

2.2 Synthesis of carbon nanotube

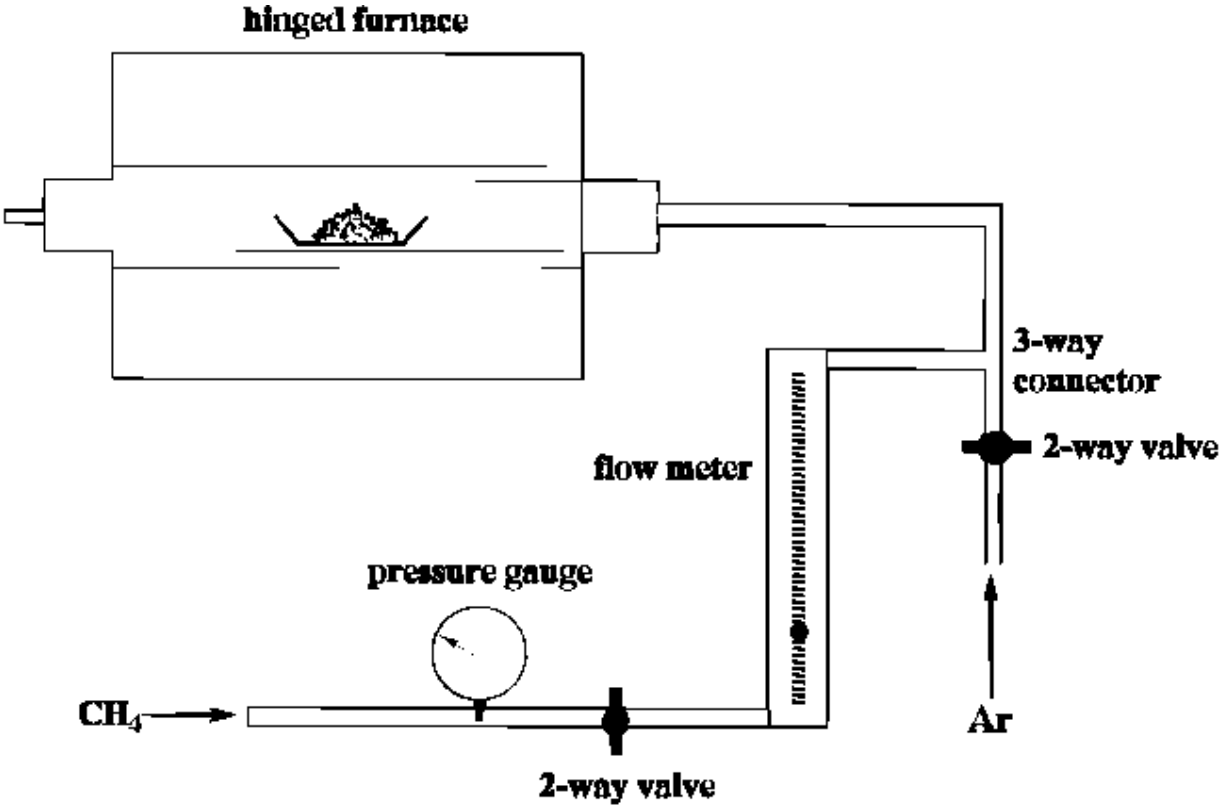

(Fig 2.3: Chemical vapor deposition setup for producing single-walled carbon nanotube)[14]

Single walled carbon nanotubes are usually produced by Chemical Vapor deposition (CVD).[14] In CVD, the substrate is exposed to one or more volatile precursors, which react and decompose on the substrate surface to produce the desired thin film deposit. Various parameters, such as the choice of reacting material, catalyst, temperature and gas flow will all affect the production of film.

The CVD growth of single-walled carbon nanotube requires a combination of carbon source and catalyst. Typical carbon sources include methane,[15]C2H4,[16] CO[17] and

CO2.[18]Metals used to catalyze CNT are most often transition metals, in particular Iron, Cobalt and Nickel. Among them, Iron catalysts can produce both MWCNT and SWCNT, while Iron-Cobalt alloys and Nickel-Cobalt alloys prefer leading to SWCNT.[19] Catalysts can be easily washed away after synthesis.

The as-synthesized carbon nanotubes usually have a distribution in diameter and chirality, containing both metallic and semiconducting CNT at the same time. Huge efforts have been put on controlling the chirality of single-walled carbon nanotube during growth, but even recent researches cannot produce CNT of the same chirality.[20][21] However, it is clear that the chirality of CNT is influenced by the composition of the reacting gas.

Since the produced CNT is usually a mixture of both metallic CNT and semiconducting CNT, the separation of these two different kinds of carbon nanotube is important. In principle, there are two ways of separating them. The first way is based on the electrical properties difference between metallic materials and semiconducting materials, including applying electric field difference in carbon nanotube solution and let the two types of carbon nanotube separate due to dielectric constant difference and burning metallic carbon nanotube by applying sufficiently high voltage,[20][21]thus metallic CNT are burnt due to much higher electrical current flowing through them.[22] The second way is separating the CNTs through their chirality difference. In this method, CNTs flow through a gel that exhibits strong interaction with carbon nanotubes that have particular chirality, and thus the selection of chirality can be achieved.[23]

2.3 Carbon nanotube electronic devices

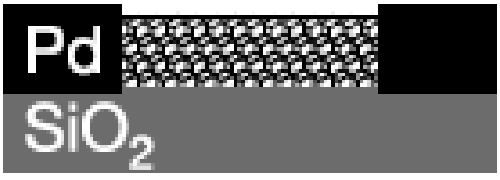

(Fig 2.4: Structure of ballistic electronic device made from carbon nanotube)[24]

Unlike typical semiconductor materials, carbon nanotube is a 1D material, which means electrons can only propagate and be reflected back in one direction. Early researches have shown that semiconducting carbon nanotube can exhibit great charge carrier mobility and can be made into ballistic electronic devices. Ballistic electronic devices refer to electronic devices where the mean free path of charge carrier is larger than the length of the device. In this case, the conductance of charge carrier could be as high as $\frac{2e^2}{h}$, where h is the Plank constant. Ballistic electronic devices made from carbon nanotubes have demonstrated superior electron conductivity and thermal conductivity experimentally and show similar I-V characteristics to traditional semiconductor electronics.[25]–[28] It is estimated that the mean free path of single-walled carbon nanotube is larger than 1μm.

Carbon nanotubes are usually p-type materials in air since they are easily partially oxidized. They can also be turned into n-type semiconductor by introducing dopants, and p-n junctions can be fabricated.[29] However, the n-doped carbon nanotubes are usually unstable. Therefore, field effect transistors (FETs) that require no doping (like MODFET) could be a better choice for the fabrication of electronic devices of carbon nanotubes.

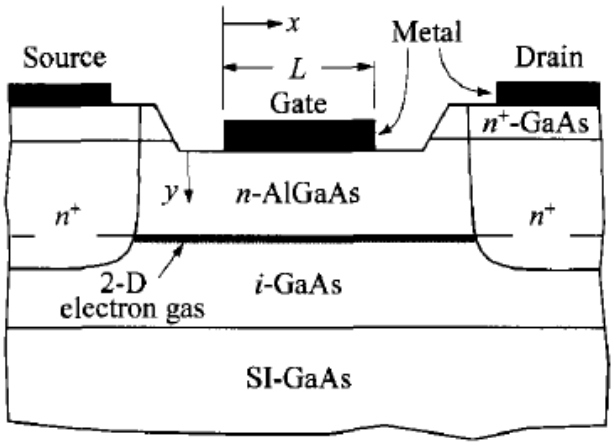

(Fig 2.5: Structure of a typical AlGaAs/GaAs MODFET)[30]

The structure of a typical AlGaAs/GaAS MODFET is demonstrated in Fig 2.5 for a comparison with carbon nanotube field effect transistors. This device functions by controlling the conduction of the channel, which is a thin interface area between the n-AlGaAs and the i-GaAs containing two dimensional electron gas (2DEG). Since 2DEG has relatively high conductance, the electric current mainly flows through this area when the device is functioning. The conductance of the channel is controlled by the gate, which is an oxide contact that controls the cutting-off of the current by applying different electrical field. Since 2DEG results from both piezoelectrical effect and quantum confinement, the AlGaN layer on top is n-doped so that more electrons can flow into the 2DEG channel. The semiconducting area underneath the source and drain side are heavily dope for enhancing conductivity. These devices demonstrate ultra high speed due to the high electron mobility of 2DEG and the confinement of electron conduction in the 2DEG channel.

The structure of MODFET can give a hint on the fabrication of carbon nanotube field effect transistors. Carbon nanotubes can naturally function as a confined channel due to its 1D structure, and the channel can be much smaller. More freedom is allowed for the choice of substrate since no phase segregation or threading dislocation need to be considered.

However, the alignment of the carbon nanotubes becomes a potential problem. All the ballistic electronic devices in previous researches are made by one single carbon nanotube, and the total current flow through them is limited. However, it is no easy task to fabricate CNT devices in a large scale since it is hard to get all the carbon nanotubes aligned in one direction. Without special treatment, the deposited carbon nanotube film is randomly aligned and aggregation of carbon nanotubes, which means several carbon nanotubes gather together as a rope, usually occurs. Previous researches have shown that crossing carbon nanotube junctions and carbon nanotube aggregations may cause a variation in conductivity.[31][32] Therefore, aligning carbon nanotubes is very important.

One method of aligning carbon nanotubes is depositing catalyst in an arrayed way. Arrayed carbon nanotubes can be automatically grown on SiO2 substrates during CVD growth, but the existence of metallic carbon nanotubes becomes a problem.[33] Another way is to obtain aligned carbon nanotubes is to use special treatments to get CNTs aligned during the deposition of its solution. One of the methods is to use a polymer membrane. By dissolving the polymer modulus afterwards, a well-aligned array of carbon nanotubes can be obtained. In this way, the diameter of the carbon nanotubes can also be selected.[34]The alignment of carbon nanotubes can also be achieved through the selection chirality [35] and through solution shearing procedure.[36]

In conclusion, there is still a long way to go for carbon nanotubes to commercialized. It is suggested in the ITRS Roadmap for semiconductors [37] that the obstacles faced by carbon nanotubes are:

- Synthesis CNT with tight distribution of bandgap and mobility;
- Characterization of electrical properties of embedded nano contact interfaces;
- CNT with low resistance contacts on both ends;
- Manufacturing and purification methodologies of CNT to achieve required purity levels (pure semiconductor with bandgap);
- Synthesis or assembly of CNTs in predefined locations and directions with controlled diameters, chirality and site-density;
- Control defects in carbon nanotubes;

It is also suggested that a combination of computer simulation and experimental characterization will enhance the efficiency of probing the defects on carbon nanotubes.

3. Finite Element Method Simulation

3.1 Introduction to Finite Element Method simulation and COMSOL

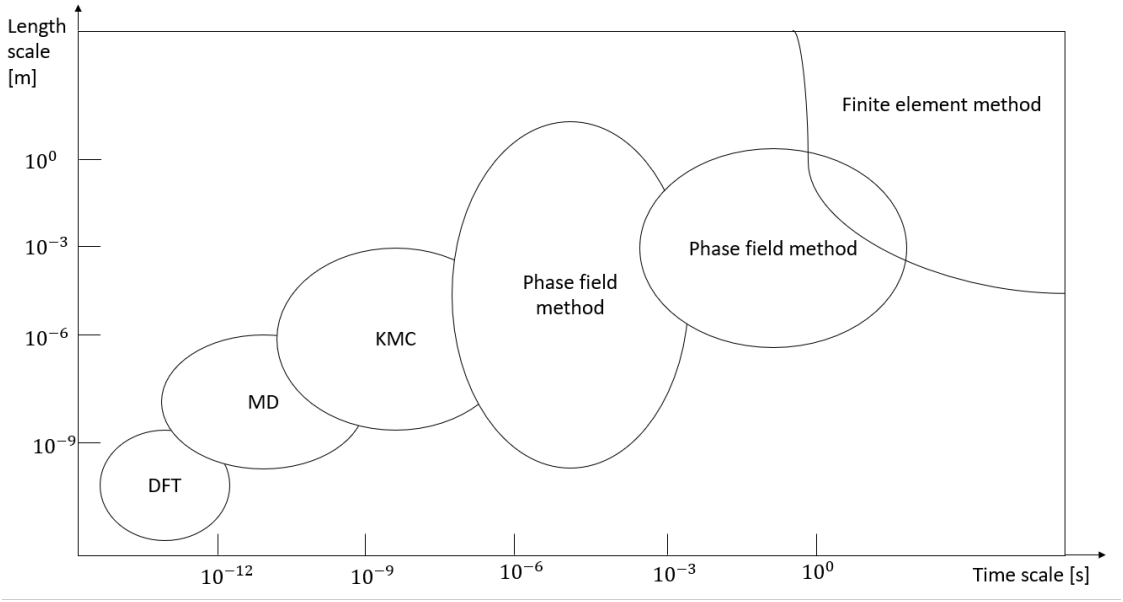

(Fig 3.1: Application range of different calculation methods)

Computer simulation is applied in this thesis for an assistance in setting up characterization goals. Typical ways of simulation include density function theory calculation, MD, KMC, phase field calculation, transport theory and finite element method simulation. However, all of these simulation methods have a limitation of cases they are suitable for, as is shown in Fig 3.1. For an electronic device that has a length of 1μm and operate for a time over 1s, finite element method (FEM) is the best choice for its simulation. Previous research also shows that FEM gives out good result for SWCNT electronic device simulations.[38]

Finite element method (FEM) simulation is a numerical method for solving problem of engineering and mathematical physics by subdividing the large system into smaller, simpler shaped parts. These smaller parts are called finite elements. After setting up boundary conditions for the system, FEM then uses variational methods from the calculus of variations to approximate a solution by minimizing an associated error function.

Therefore, a correct simulation requires both a correct setup of physical boundary conditions and a good convergence. There are two ways to test whether a correct simulation result is given or not. The first way is to see whether a good convergence is given or not, and the second way is to perform calculation for several times to see whether the results are identical.[39]Both of these methods are applied in this research.

COMSOL Multiphysics is used here to perform FEM calculation. COMSOL MultiPhysics is a commercial software that performs FEM simulation on multi-physical problems using Matlab.[40]In this research, COMSOL is used to simulate the DC performance of a field effect transistor with well-aligned nanotube and probe the effect of random alignment of carbon nanotubes on its performance. The setup of physical model is discussed below.

3.2 Model setup and boundary conditions

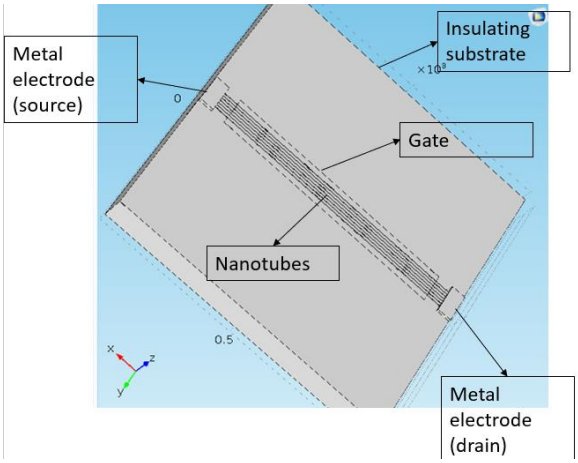

(Fig 3.2: Model setup of arrayed nanotube simulation)

In this model silicon nanowires with bandgap, carrier density and carrier mobility changed to CNT's used for latter experiment are used to simulate SWCNT, while other parameters were not changed due to a lack of data. The bandgap of these nanotubes is set to be 0.95 eV according to the Raman Results discussed in the next section. Carrier mobility is set to be 10^5 and the electron density is set to be $5\text{x}10^{23}$. For simplification of setting up different boundary conditions on different faces, these nanotubes are set to be cubic rather than round.

The model simulated is a back-gated field effect transistor. It consists of an oxide substrate, seven nanowires, two metal electrodes (source and drain) and an oxide gate, as is shown in Fig 3.2. The boundary conditions are discussed below.

Boundary conditions

A combination of semiconductor equilibrium study and stationary study is used for simulation. Stationary study simulates the condition where field variables do not change over time, which is suitable for solving DC performance of electronic devices. However, preset initial value is needed for performing this study since a good convergence is hard to be obtained with this study alone. Semiconductor equilibrium study is used to obtain a preset initial value here. Semiconductor equilibrium study assumes that the system is under thermal equilibrium and only Poison's equilibrium is solved in this case. These two studies differ a little bit in their boundary conditions.

Physical conditions for bulk nanotubes

All the nanotubes are set to follow the semiconductor material. Therefore, all the nanotubes are considered to follow continuation equation.

Semiconductor equilibrium	Stationary
$\nabla \cdot (-\epsilon_r \nabla V) = \rho$ $\rho += q(p - n + N_d^+ - N_a^+)$ $\nabla \cdot J_n = 0$ $\nabla \cdot J_p = 0$ $J_n = qn\mu_n \nabla E_c + \mu_n k_B T G \left(\frac{n}{N_C}\right) \nabla n + qnD_{n,th} \nabla \ln(T)$	$\rho += q(p - n + N_d^+ - N_a^+)$ $\nabla \cdot J_n = 0$ $\nabla \cdot J_p = 0$ $J_n = qn\mu_n \nabla E_c + \mu_n k_B T G \left(\frac{n}{N_C}\right) \nabla n + qnD_{n,th} \nabla \ln(T)$

$J_p = \mathrm{qn}\mu_p \nabla E_v - \mu_p k_B T G \left(\frac{p}{N_v}\right) \nabla p$ $- qpD_{p,th} \nabla \ln(T)$ $E_c = -(V + X_0)$ $E_v = -(V + X_0 + E_{g,0})$	$J_p = \mathrm{qn}\mu_p \nabla E_v - \mu_p k_B T G \left(\frac{p}{N_v}\right) \nabla p$ $- qpD_{p,th} \nabla \ln(T)$ $E_c = -(V + X_0)$ $E_v = -(V + X_0 + E_{g,0})$

(Table 3.1: Comparison of boundary conditions between semiconductor equilibrium and stationary setup)

Source and drain

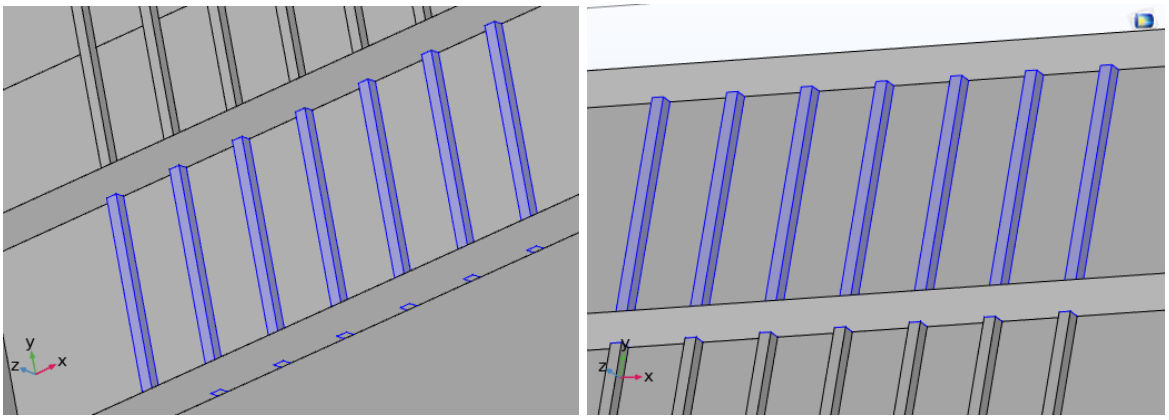

(Fig 3.3: Source (left) and Drain (right) area of arrayed nanotube FET that metal-semiconductor boundary conditions are spplied on)

The contacts of nanotube to the metal in source and drain are set to be ideal Ohmic metal contact for simplification. As is shown in Fig 3.3, only three sides of the nanotube are in contact with metal are considered to follow this boundary condition, and the back side in contact with the substrate is set to insulating. The physical conditions of the metal-semiconductor contact are:

Semiconductor equilibrium	Stationary

$\mathrm{V} = V_{eq} + V_{0,bias}$	$\mathrm{V} = V_{eq} + V_0$ $\mathrm{n} = \frac{1}{2}(N_d^+ - N_a^-) + \frac{1}{2}\sqrt{(N_d^+ - N_a^-)^2 + 4\gamma_n\gamma_p n_{i,eff}^2}$ $\mathrm{p} = -\frac{1}{2}(N_d^+ - N_a^-) + \frac{1}{2}\sqrt{(N_d^+ - N_a^-)^2 + 4\gamma_n\gamma_p n_{i,eff}^2}$

(Table 3.2: Boundary conditions for ideal ohmic contact)

Gate

The gate is set to be ideal insulator gate that permits no charge transfer with no tunneling. The boundary condition is set as:

Semiconductor equilibrium	Stationary
$\mathrm{n} \cdot \mathrm{D} = \frac{\epsilon_{ins}\epsilon_0}{d_{ins}}(V + \emptyset - V_0 + V_{eq,adj})$ $\mathrm{n} \cdot J_n = 0$ $\mathrm{n} \cdot J_p = 0$	$\mathrm{n} \cdot \mathrm{D} = \frac{\epsilon_{ins}\epsilon_0}{d_{ins}}(V + \emptyset - V_0 + V_{eq,adj})$ $\mathrm{n} \cdot J_n = 0$ $\mathrm{n} \cdot J_p = 0$

(Table 3.3: Boundary conditions for ideal gate contact)

Boundary conditions for all other interfaces

All the other interfaces are considered to be insulating, which means no current flow is allowed. The equations for them are:

Semiconductor equilibrium	Stationary
$\mathrm{n} \cdot (D_1 - D_2) = 0$ $\mathrm{n} \cdot J_n = 0$ $\mathrm{n} \cdot J_p = 0$	$\mathrm{n} \cdot (D_1 - D_2) = 0$ $\mathrm{n} \cdot J_n = 0$ $\mathrm{n} \cdot J_p = 0$

(Table 3.4: Boundary conditions for insulating interfaces)

3.3 Results and discussions

COMSOL simulation is shown to be able to demonstrate the distribution of electron density, hole density and electric field distribution of well-aligned nanotube FET, as is shown in Fig 3.4. It can be seen that most of the electric field and charge carrier concentration variation happens at boundary between the source side and the gate side. I-V_d curve (Fig 3.5) and I-V_g curve (Fig 3.6) were also drawn. It is clear that the I-V_d curve shows a typical performance as an FET after V_d<-0.6V and the I-V_g curve shows good gate modulation. The conclusion of this simulation is similar to experimental measurement in [12].

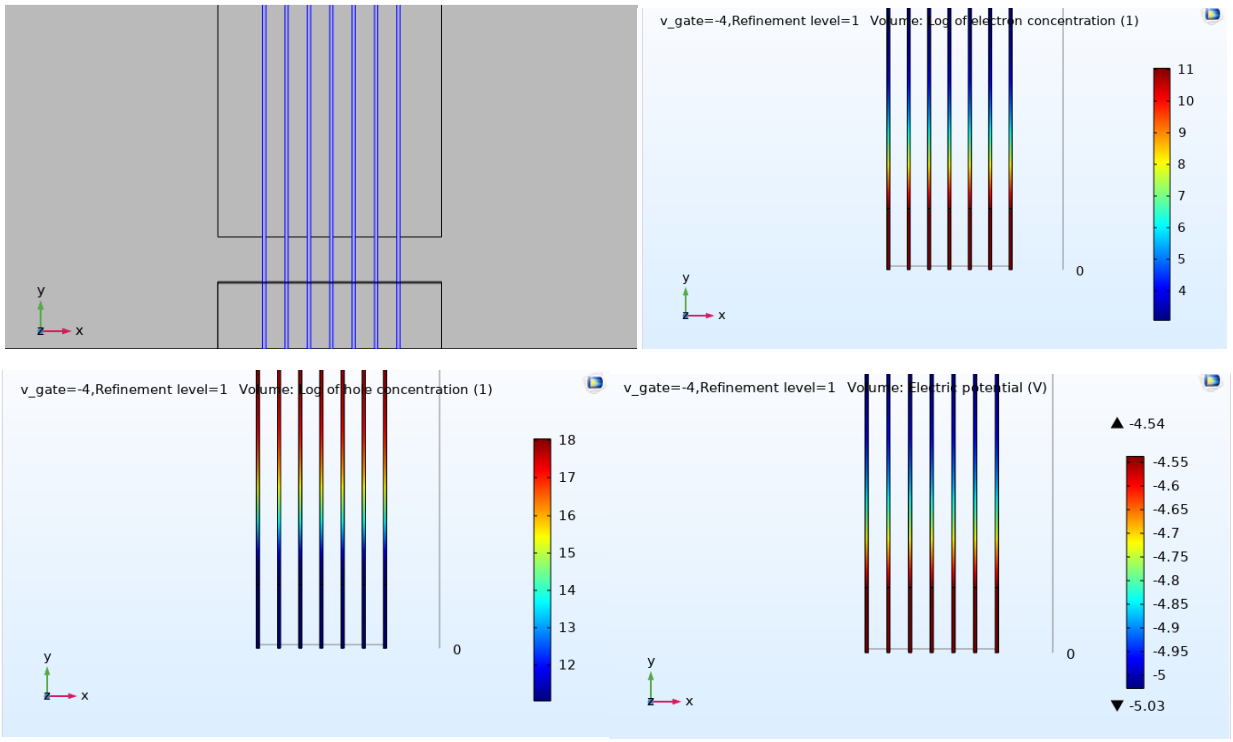

(Fig 3.4: Simulation results on the source area of the well-aligned nanotube FET)

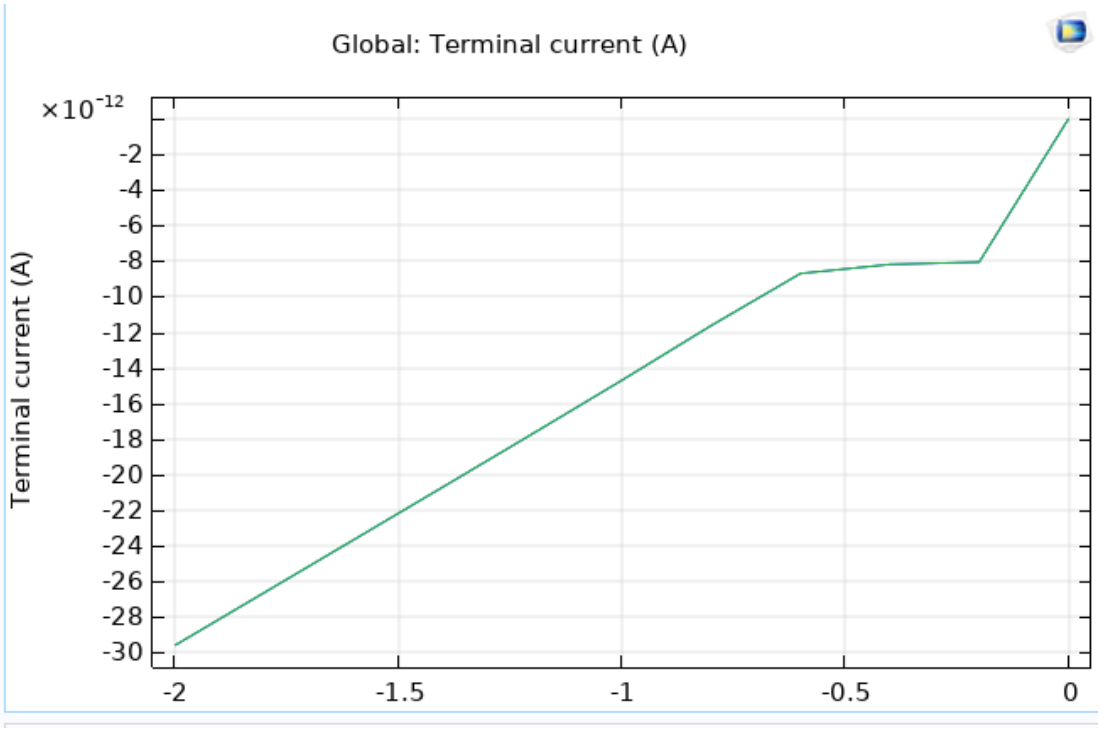

(Fig 3.5: Simulated I-V_d curve of well-aligned nanotube FET)

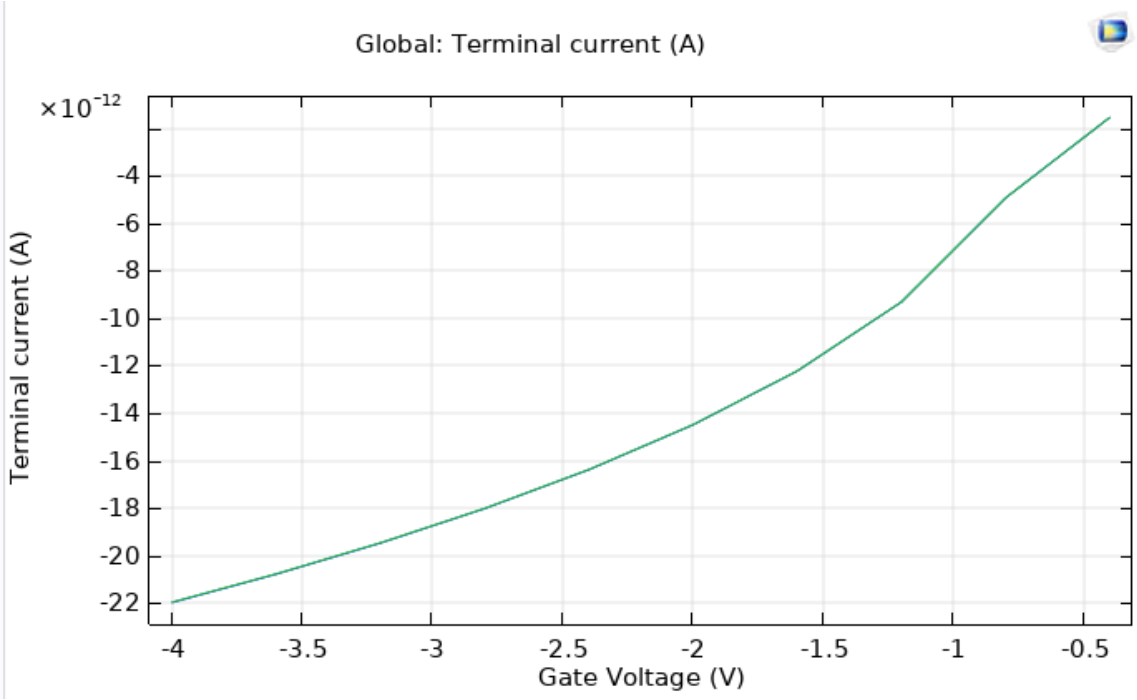

(Fig 3.6: Simulated I-V_g curve of well-aligned nanotube FET)

Simulation on the effect of not well-aligned nanotube on well-aligned nanotube FET

COMSOL is used to probe the effect of the existance of not well aligned nanotube on a well-aligned nanotube FET. In this model, a single crossing nanotube is in contact with all the other carbon nanotubes on the surface, and all the other settings are the same as the well-aligned nanotube FET. The setup is demonstrate in Fig 3.7. To testify the validity of the simulation results, simulation was done for three times and good convergence was observed, as is shown in Appendix. Therefore, it is assumed that the results are reasonable.

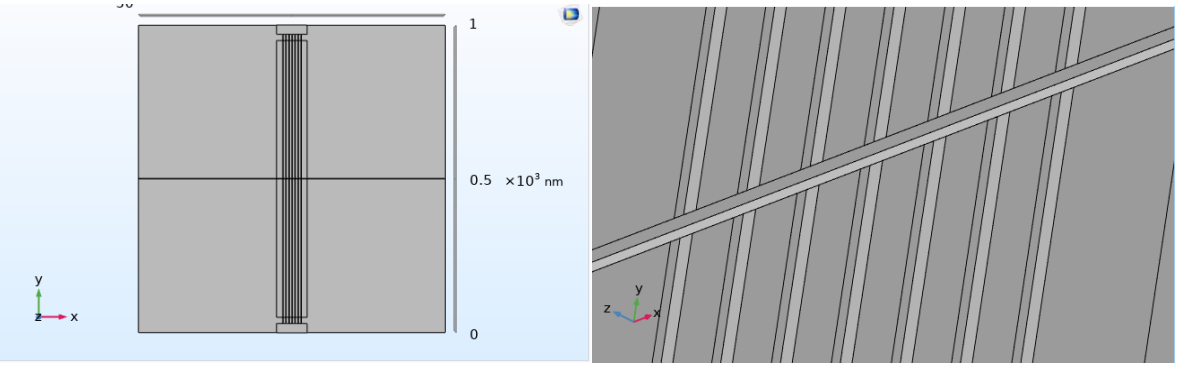

(Fig 3.7: Setup of the simulation model for well-aligned nanotube FET with crossing nanotube ontop and detailed structure of the crossing area)

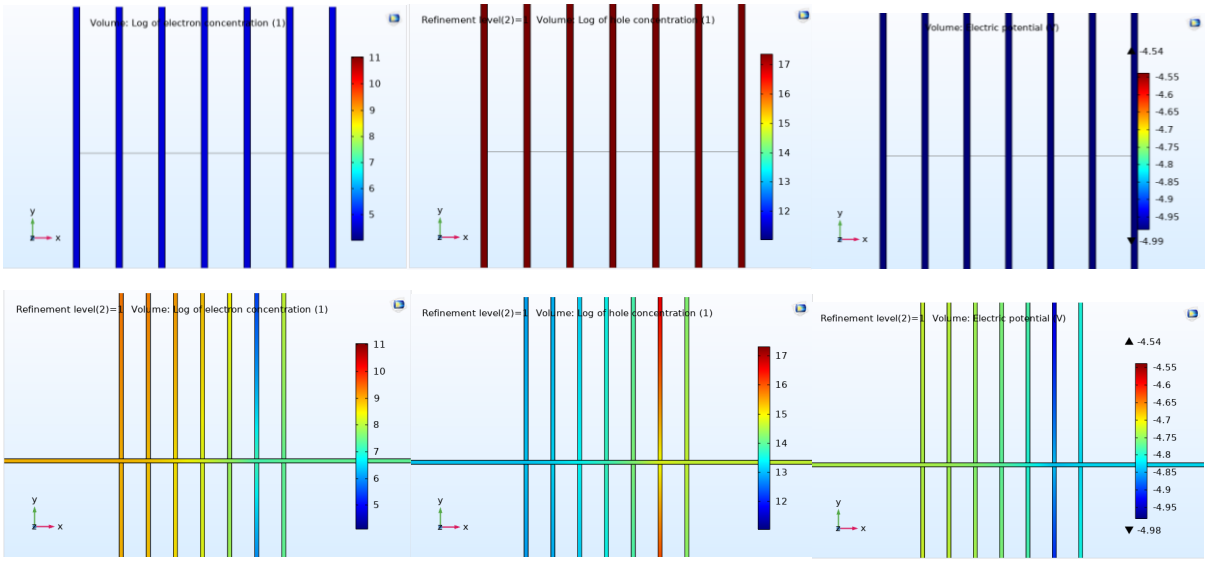

(Fig 3.8: Electron distribution, hole distribution and electric field distribution of well-aligned nanotube FET (top) and the one with crossing nanotube on top (bottom) at V_d =-0.1, V_g =-1.5)

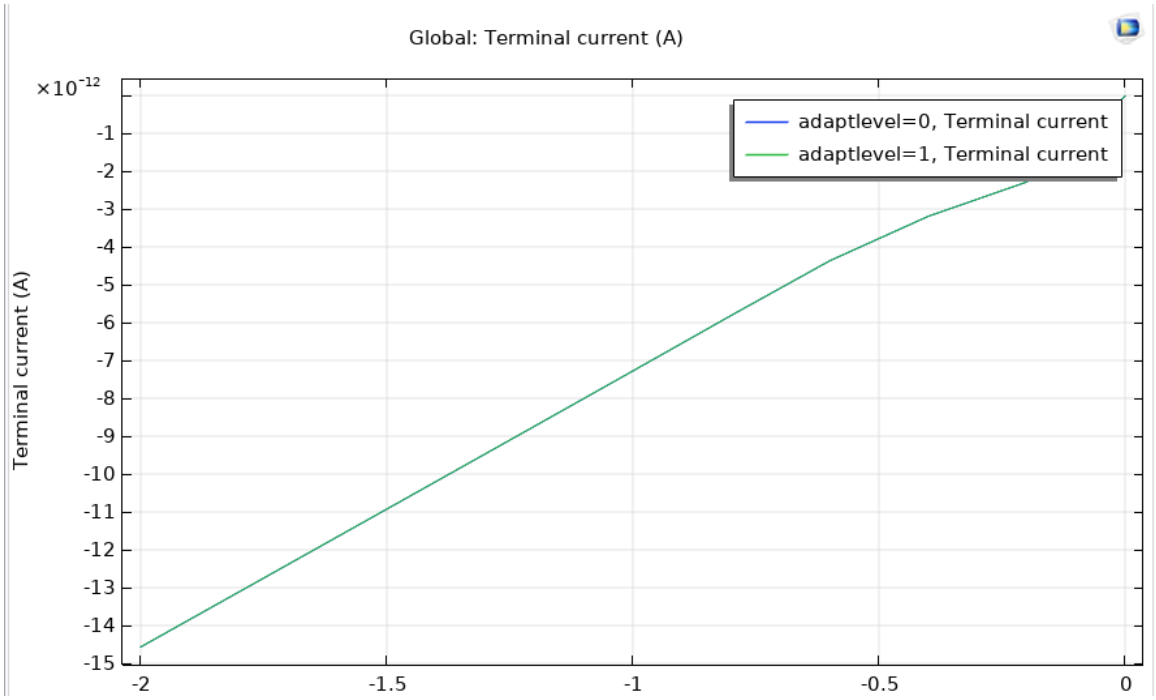

(Fig 3.9: I-V_d curve simulation of well-aligned nanotube FET with crossing CNT on top when V_g =-1V and V_s=0V)

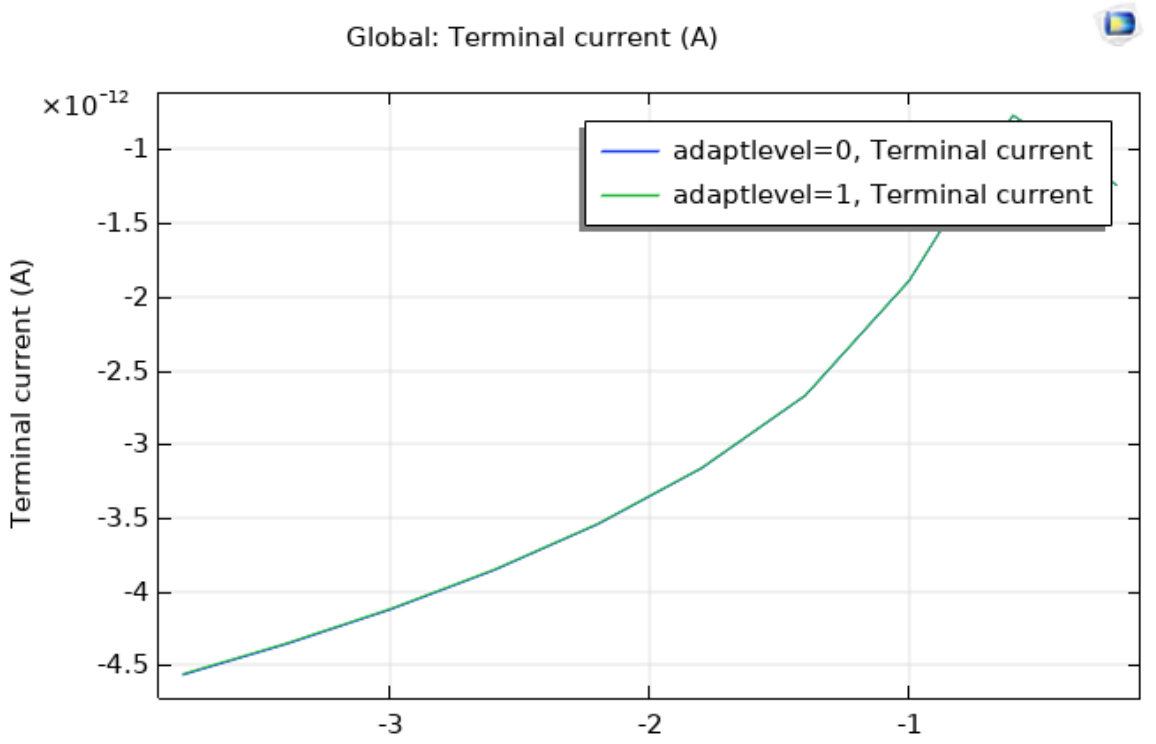

(Fig 3.10: I-V_g curve simulation of well-aligned nanotube FET with crossing nanotube on top when V_d =-0.1V and V_s =0V)

As is shown in Fig 3.8, if a single nanotube is lying on an array of nanotubes, the electric field will concentrate on one single nanotube of the arrayed nanotubes, which will cause a concentration of electrical current. This could lead to a local burning of carbon nanotubes during high power operation since only a single carbon nanotube is carrying electrical current. Therefore, it is important to characterize the alignment of carbon nanotubes to see whether misaligned carbon nanotubes exist. I-V_d curve (Fig 3.9) and I-V_g curve (Fig 3.10) was also calculated. It can be seen that a single misaligned nanotube will lead to a significant decrease of the total current flow through the device.

4. Experimental Method

4.1 Raman Spectroscopy and Raman Imaging

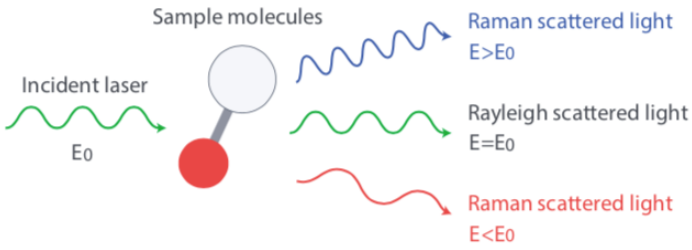

(Fig 4.1: Mechanism of Raman Scattering)[41]

Raman Spectroscopy is a useful tool for probing the structure of a material by measuring the inelastic scattering of photon by phonon of the material. In Raman spectroscopy, laser beam is used to excite electrons from valence band to conduction band and remitted light is collected. Some of the excited electrons are inelastically scattered by phonons before falling back to the valence band, and thus create a difference in frequency between the inlet photon and the outlet photon. This phenomenon is called Raman effect. Since the energy difference is created through the scattering of phonon, Raman signals can be used to reveal the structure of the material. Raman spectra is affected by both the wavelength of laser and the temperature.

Based on the number of electrons involved, there are two types of Raman Scattering process: 1st order and 2nd order process. In 1st order process, only one electron is involved in scattering. However, in 2nd order process, scattering happens for two electrons. 2nd order Raman scattering process usually has lower intensity compared with 1st order, but is useful in detecting defects on the structure.

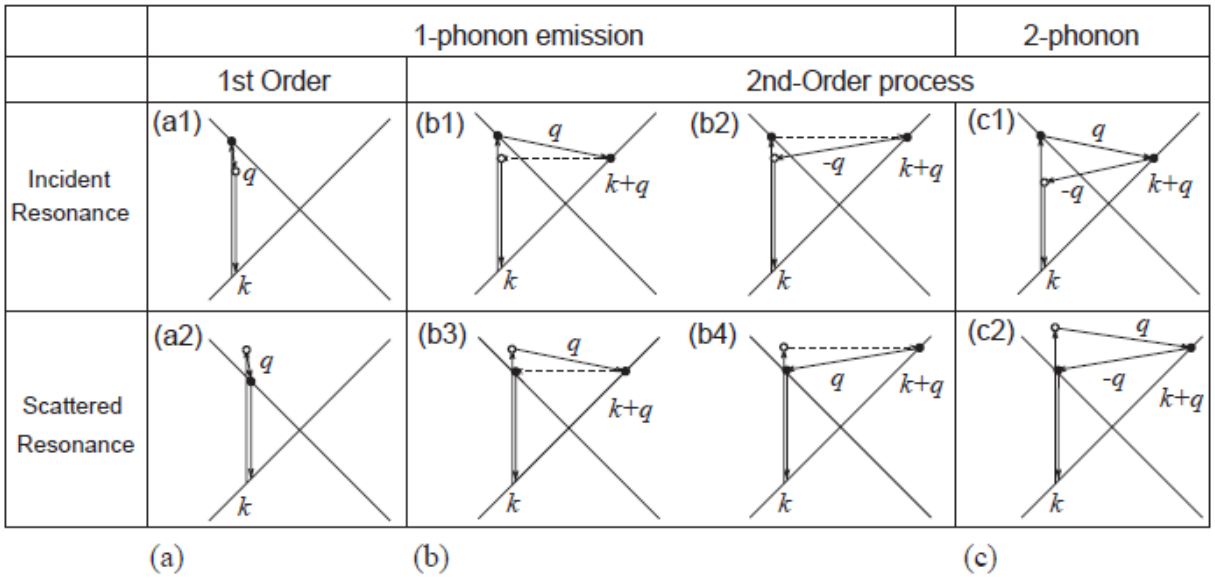

(Fig 4.2: 1st order and 2nd order process)[42]

Raman spectroscopy is widely used for characterizing carbon nanotubes. It can be used to reveal the diameter, the electrical properties (whether the carbon nanotubes are metallic or semiconducting), and defects of carbon nanotubes. Typical Raman peaks are shown in Fig 4.3.

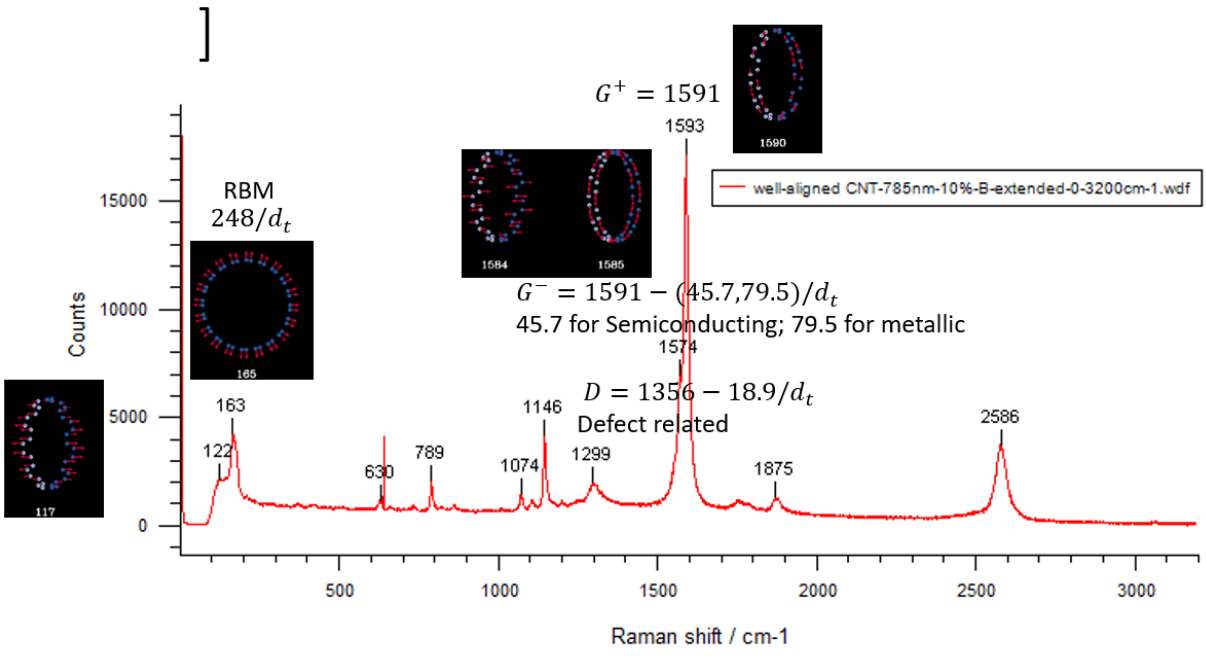

(Fig 4.3: Typical Raman spectroscopy of SWCNT, vibration modes cited from [43])

Radio breathing mode

Radio breathing mode (RBM) denotes the coherent vibration of the C atom in the radial direction, as if the tube is breathing.[42] RBM occurs in a frequency range of 120-350cm^{-1} for nanotube with a diameter of 0.7nm-2nm. This mode is usually used to characterize the diameter of CNT. The association between the diameter of CNT and the RBM peak is $248/R_t$, where R_t is the diameter of the carbon nanotube.

G band

G band is the peak at ~1591cm^{-1}, which originates from the vibration of the C-C band along the nanotube direction. This peak has a high Raman intensity and is a good indicator of the existence of carbon nanotubes. However, since G band indicates the C-C bond, it also exists for graphene,[44] so other peaks need to be considered for determine the band is graphene, such as the G' band.

G' band

G' band is the Raman peak around 1570 cm^{-1}, which is associated with the vibration along the circumferential direction along the CNT. This band is also very strong, and it is a good indicator of whether the material is carbon nanotube or other types of carbon materials. Example will be shown in the result part.

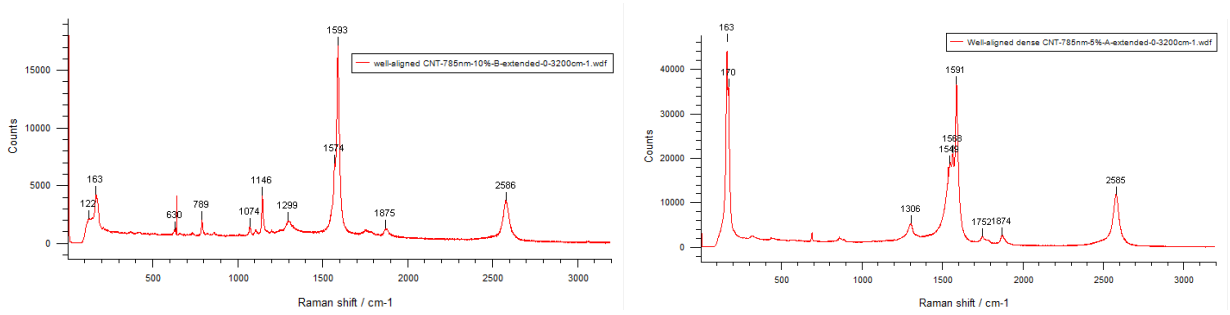

(Fig 4.4: Raman Spectra of semiconductive CNT (left) Metallic CNT (right))

The shape of Raman Spectra is the way to tell whether a SWCNT is semiconducting or metallic. In Fig 4.4, the sample of spectra A contains mostly semiconducting carbon nanotubes, while the sample on the right contained both semiconducting and metallic CNTs. It can be seen that for samples with mostly semiconducting CNT, the RBM intensity is low and the G and G- band can be tell apart, while sample containing metallic CNT is the opposite.

D band

D band denotes the vibration peak around 1300 cm^{-1}. This peak is associated with a destruction of symmetry of graphene structure since carbon nanotube is a rolled up of graphene. D band is related to secondary Raman scattering of carbon nanotube. Some researches have shown that a change in the intensity of D band is associated to the destruction of carbon nanotubes.[45]−[47]

Raman Imaging

Aside from obtaining Raman Spectra at one spot, scanning laser can also be used for obtaining Raman signals, which is called Raman Imaging. The mechanism of Raman imaging is the same as SEM, only substituting electron beam with laser beam. This technique proves to be useful in revealing the structure of materials. However, due to Rayleigh's law, the resolution of this technique is about 200nm.

In this technique, Raman Signal is collected at all the scanned sites of the sample. Image are formed by data processing. In this work, images are formed by summing the intensity over a wavelength area. As is shown in Fig 6B, every point in the picture is the integration of the Raman intensity over 1550-1620 cm^{-1}.

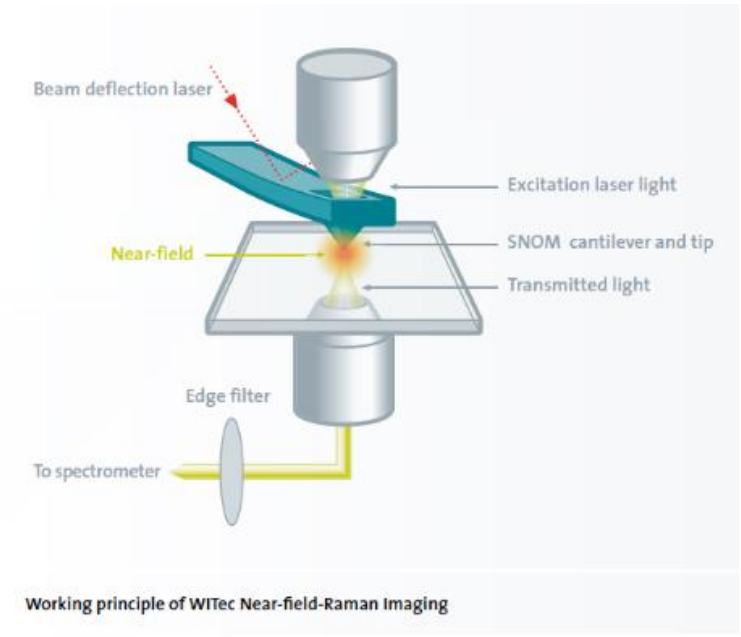

(Fig 4.5: Structure of Raman imaging system)[48]

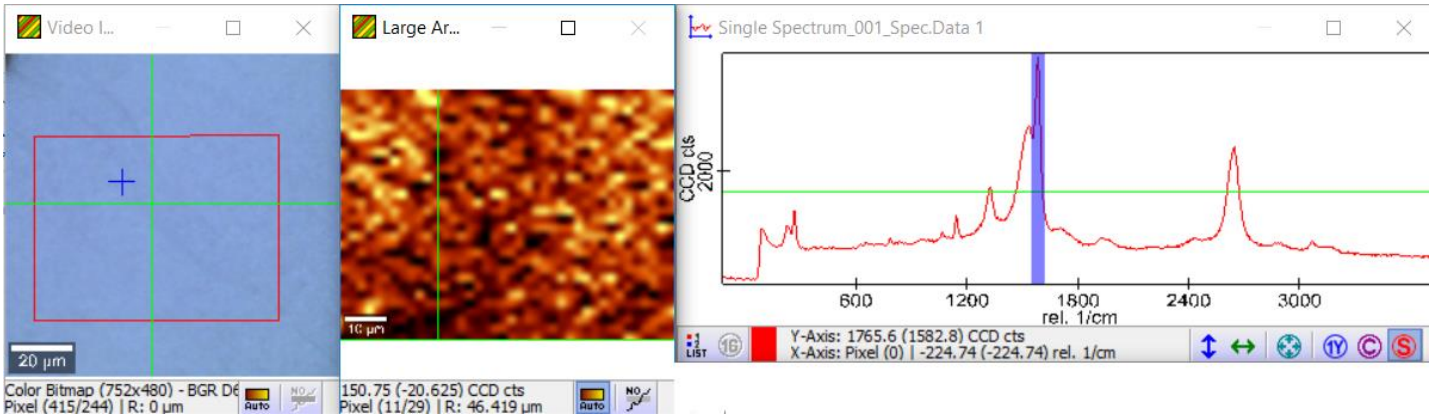

(Fig 4.6: A: Setup of Raman Imaging: Image forming technique)

The quality of the Raman imaging is limited by the cycle time, which is the time the laser spot stays at each point. A longer cycle time would slow down the scanning speed, but a too short cycle time would not lead to a failure in collecting enough Raman signal. In Raman imaging, a long time Raman signal is first obtained at one spot for reference. Then the user can manually adjust the staying time by collect Raman signal at a single spot for different time to find out the suitable staying time which is long enough to collect a tolerable Raman signal.

4.2 Scanning Electron Microscopy

Scanning Electron Microscope (SEM) is a widely used method of imaging nanometer scale structures. A typical SEM is composed of electron guns, electron lenses, spray aperture, scan colls and the detector. During the operation of SEM, electrons come out of the electron gun is first focused by the electron lenses, filtered by the aperture, and then differed by the scan colls to scan on the sample. Signals are collected by detector to form image.

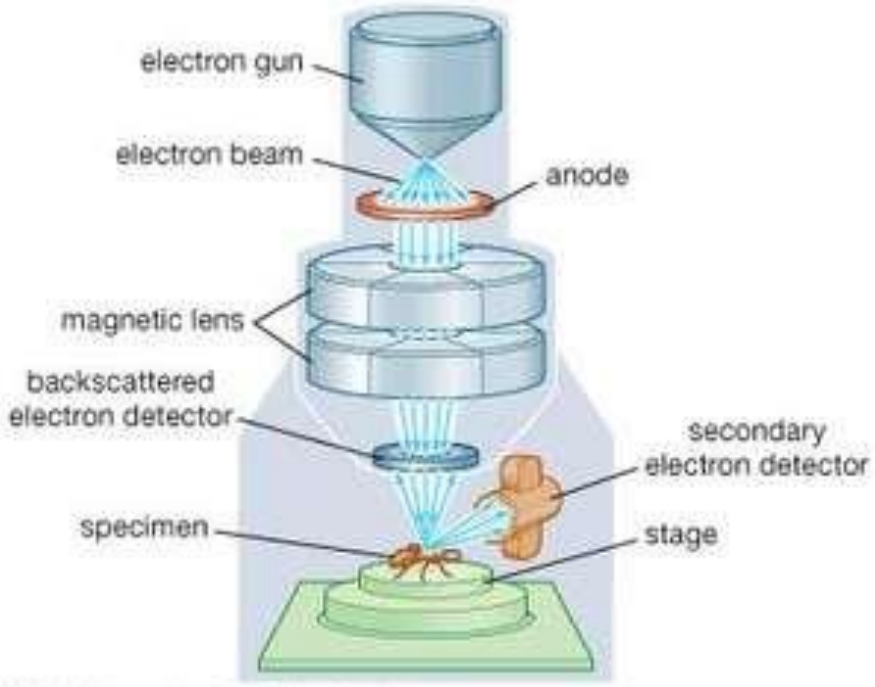

(Fig 4.7: Structure of SEM system)[49]

One of the most collected signals is secondary electron. Secondary electrons are electrons generated by other radiations that occurs when inlet electrons knock off inner shell electrons of an atom. Since secondary electrons usually have a low energy, the sampling volume is low and surface morphology can be better imaged. Therefore, secondary electron imaging is widely used for imaging fine structures.

The ultimate resolution of the SEM is defined as the smallest probe size which can provide an adequate signal from the specimen.[50] The probe size might be decreased by increasing the strength of the condenser and decreasing the working distance. Theoretically, the probe diameter is

$$d_g = [d_g^2 + d_s^2 + d_d^2 + d_c^2]^{1/2}$$

Where the probe size d_g

$$d_g = \sqrt{\frac{4 \cdot i_p}{\pi^2 \cdot B \cdot \alpha^2}}$$

the probe current

$$i_p = \frac{B \cdot \pi^2 \cdot \alpha^2 \cdot d_g^2}{4}$$

The brightness

$$B = \frac{J_c \cdot e \cdot E_0}{\pi \cdot k \cdot T}$$

The diameter if the disk of least confusion

$$d_s = 2 \cdot C_s \cdot \alpha^3$$

The chromatic aberration

$$d_c = \frac{1.21 \cdot \lambda}{\alpha}$$

(α *is aperture angle,* B is theoretical brightness, J_c is current density on the cathode, e is electron charge, k is Boltzman constant, T is absolute temperature.)

Among these parameters, chromatic aberration is inherent to the electron gun and cannot be changed. Therefore, to achieve the maximum SEM resolution, probe diameter, aberration, contrast, brightness and working distance are the parameters that we should adjust.

The resolution of SEM is also affected by the conductivity of the sample. If the sample is not that conductive, electron will accumulate on the surface of the sample, which lead to a blurred image or damage of the sample. This is called charging effect. Typical ways of improving conductivity of sample are depositing a layer of gold or applying conductive paint rather than conductive tape.

4.3 Atomic Force Microscopy

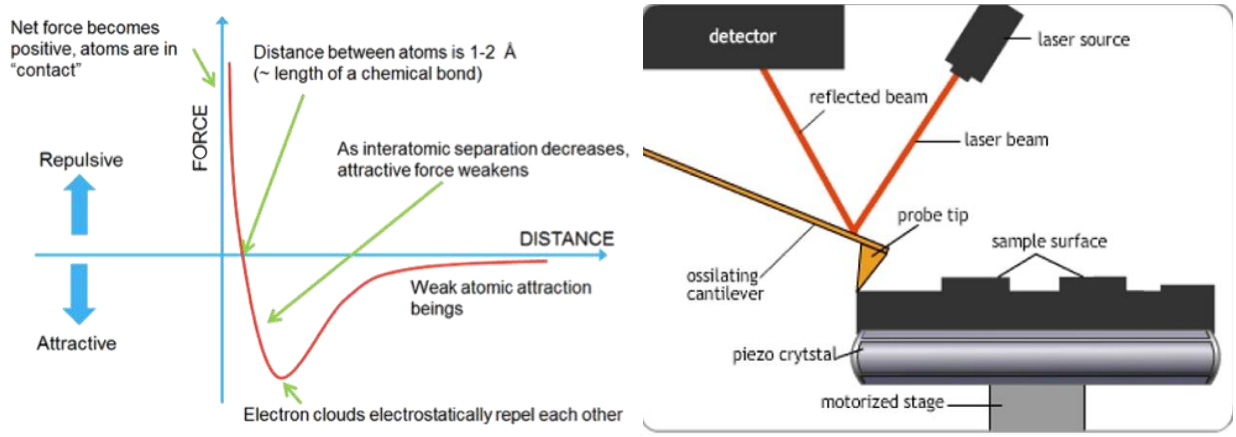

(Fig 4.8: A: Atomic Force B: Mechanism of AFM)

Atomic Force Microscopy (AFM) is a high-resolution scanning probe microscopy which uses atomic force for imaging sample surface. When AFM is performing, the AFM tip is in close contact with the surface of the sample, and a beam of laser is shot on the tip. By measuring the movement of the reflection of the laser spot, the movement of the tip can be measured, and thus the surface of the sample is recorded. The sharp AFM tip is connected to the system through a cantilever. The resolution of AFM can go down to a few nanometers.

There are three types of AFM modes for regular height imaging: tapping mode, continuous mode and ScanAnalysis mode. The difference between them lies in how the tip is in contact with the sample. In tapping mode, the tip is not always on the sample, but constantly tapping on the surface when scanning. This mode is suitable for soft materials such as polymer but may not have a very good resolution. In continuous mode, the tip is always in contact with the surface. This mode is more suitable for surface with higher modulus since it may cause damage for softer samples. ScanAnalysis mode is relatively new and can be seen as a combination of tapping mode and continuous mode. In ScanAnalysis mode, the tip is always in close contact with the surface while scanning, but tapping mode is used when the tip comes across large variation of height on the surface. Also, since the operation of ScanAnalysis mode is automatically controlled by the computer, it is much easier in operation. High resolution can also be obtained in ScanAnalysis mode.

No matter which mode is used, the resolution of AFM image is determined by the radius of the tip. The best resolution of AFM imaging is a few nanometers larger than the radius of the tip. The radius of the tip ranges from a few nanometers to tens of nanometers. The material of the tip also affects the quality of the image.

Aside from pure morphology imaging, AFM can also be used to collect other information such as mechanical response and electrical information. Mechanical AFM and Electrostatic AFM are two typical advanced AFM imaging modes. In mechanical AFM imaging, Modulus and adhesion are recorded by measuring the force needed for the tip to withdraw from the sample. Adhesion AFM image is associated with not only the type of material, but also the height of the material. Thus, it is widely used for telling apart different materials on the surface of a material.

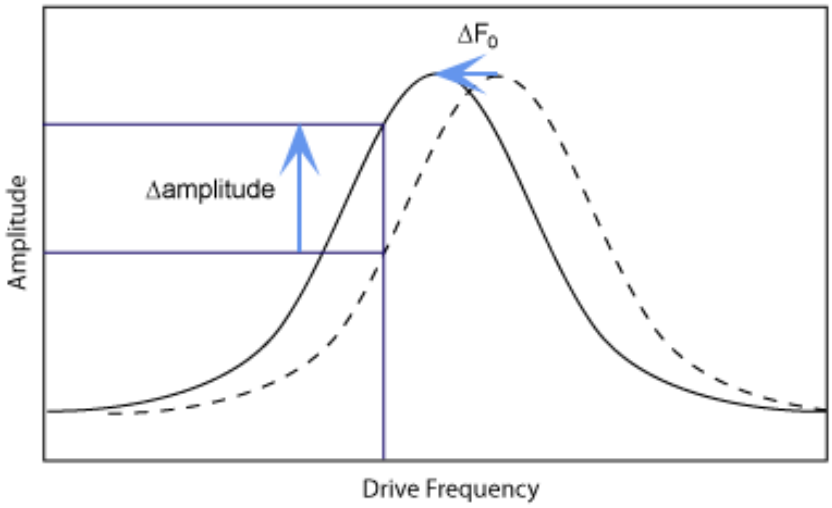

(Fig 4.9: Amplitude change in the vibration of AFM cantilever)

In electrostatic AFM, a static electric field is applied on the tip of AFM and the tip used here is conductive. The variation of surface potential can be detected by the variation of the surface potential due to electrostatic force. As is seen in Fig 4.8, when electrostatic force functions at the AFM tip, the vibration of the cantilever will change, and the amplitude of its vibration at a fixed spot will change. Thus, the change of the vibration amplitude reflects the change in surface potential. To perform this mode, the sample is required to be wired to ground. However, since a conductive AFM tip is required in this measurement, the resolution of electrical mode in AFM is usually restricted because metal coating is usually the approach for enhancing conductivity of the AFM tip. An alternate way of obtaining conductive AFM tip is using highly doped semiconductor, but these tips are usually more expensive.

5. Experimental setup

5.1 Raman Spectroscopy and Raman Imaging

In this work, Witec Near Field Raman Imaging system is used for Raman spectroscopy. The wavelength of the laser used is 633nm, and all the experiments are done at room temperature. All the spectra obtained in this thesis is done on 50X objective lens.

Raman imaging is done on RISE Raman imaging system. The cycle time is 30s and all the images are scanned only once. Laser power used is 1.009 mW.

5.2 SEM imaging

Nova 230 is used in this research for SEM imaging. The electron source is LaB6, and the resolution of this SEM can go down to 1-3nm depending on the sample. Accelerating voltage of 1-10kV are tried on the sample since higher accelerating voltage may cause destruction of carbon. Working distance of 3-5mm is adjusted for better imaging as well. Also, three ways of improving conductivity, including depositing gold, applying conductive paint and using gold electrode coated substrate are applied. Experiments are done at carbon nanotube powders (stick to conductive tape), carbon nanotubes deposited onto polymer and carbon nanotubes deposited on Si substrate with gold electrodes on top. Gold deposition is done by PLD at Chemistry department and is deposited for 30 seconds and the estimated gold thickness is around 1nm.

5.3 AFM imaging

(Fig 5.1: Bruker Dimension FastScan Scanning Probe Microscope)

Tip Specification

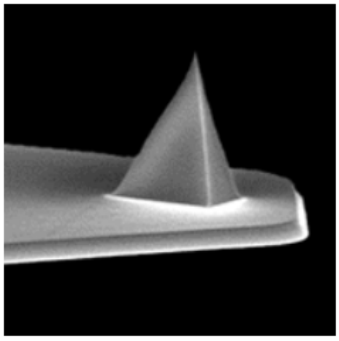

Geometry:	Rotated (Symmetric)
Tip Height (h):	2.5 - 8.0µm
Front Angle (FA):	15 ± 2.5°
Back Angle (BA):	25 ± 2.5 °
Side Angle (SA):	17.5 ± 2.5 °
Tip Radius (Nom):	2 nm
Tip Radius (Max):	12 nm
Tip SetBack (TSB)(Nom):	5 µm
Tip Set Back (TSB)(RNG):	3 - 7 µm

Cantilever Specification

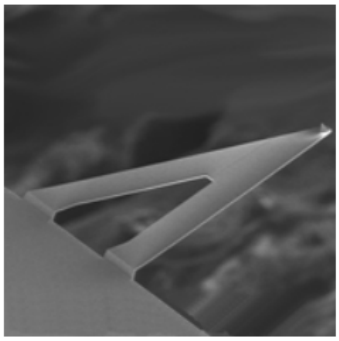

Material:	Silicon Nitride
Geometry:	Triangular
Cantilevers Number:	1
Cantilever Thickness (Nom):	0.65 µm
Cantilever Thickness (RNG):	0.6 - 0.7 µm
Back Side Coating:	Reflective Aluminum

(Fig 5.2: Basic information of the ScanAnalysis-Air tip)[51]

AFM measurement is done on Bruker Dimension FastScan Scanning Probe Microscope in Nano Characterization lab at CNSI. ScanAnalysis mode and mechanical measurement in ScanAnalysis mode are done in this research through ScanAnalysis-Air tip. The radius of the tip is 2nm, which is comparable to the diameter of our CNT sample.

Electrostatic AFM is performed through Bruker Dimension Icon Scanning Probe Microscope. This step is used to probe whether advanced electrical properties measurements, such as capacitance AFM, can be done in the future. To form a complete circuit, conductive paint is applied to connect the gold electrodes to the grounded metal plate underneath (white part on the edge in sample part). The tip used for the electrostatic AFM is SCM-PIT-V2 tip and its properties are shown in Fig 5.4. The radius of the tip is 25nm, so the resolution of the image is limited in this experiment.

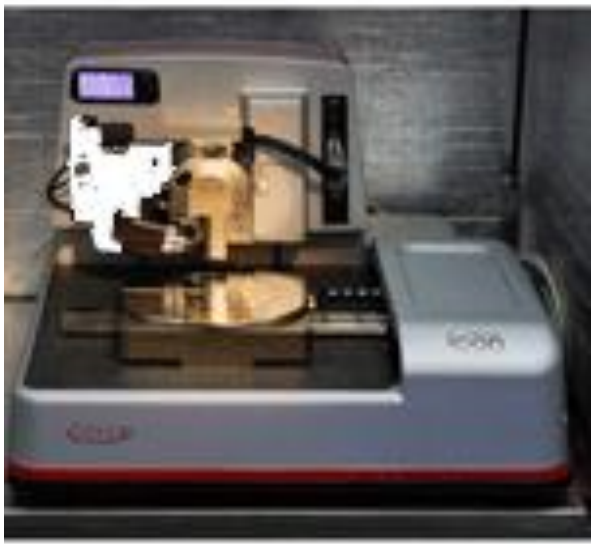

(Fig 5.3: Bruker Dimension Icon Scanning Probe Microscope)

Tip Specification

This probe uses a rotated tip to provide a more symmetric representation of features over 200nm.

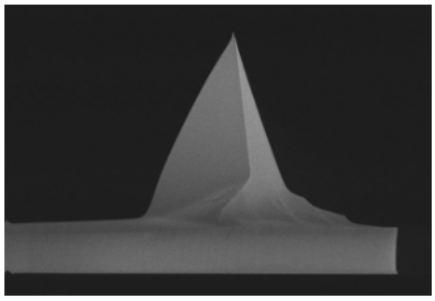

Tip Schematic

Geometry:	Rotated
Tip Height (h):	10 - 15µm
Front Angle (FA):	17.5 ± 2.5°
Back Angle (BA):	25 ± 2.5 °
Side Angle (SA):	20 ± 2.5 °
Tip Radius (Nom):	25 nm
Tip SetBack (TSB)(Nom):	9.5 µm
Tip Set Back (TSB)(RNG):	7 - 12 µm
Tip Coating:	PtIr

Cantilever Specification

The Platinum-Iridium reflective coating on the backside of the cantilever increases the laser signal (A+B) by up to 2.5 times. Although not necessary for general imaging, reflective coating is recommended for thin cantilevers (< 2.5 µm), highly reflective samples, and machine vision applications.

Cantilever schematic

Material:	0.01 - 0.025 Ωcm Antimony (n) doped Si
Geometry:	Rectangular
Cantilevers Number:	1
Cantilever Thickness (Nom):	2.80 µm
Cantilever Thickness (RNG):	2.05 - 3.55 µm
Front Side Coating:	Conductive PtIr
Back Side Coating:	Reflective PtIr

(Fig 5.4: Basic information of SCM-PIT-V2 tip)[52]

Sample

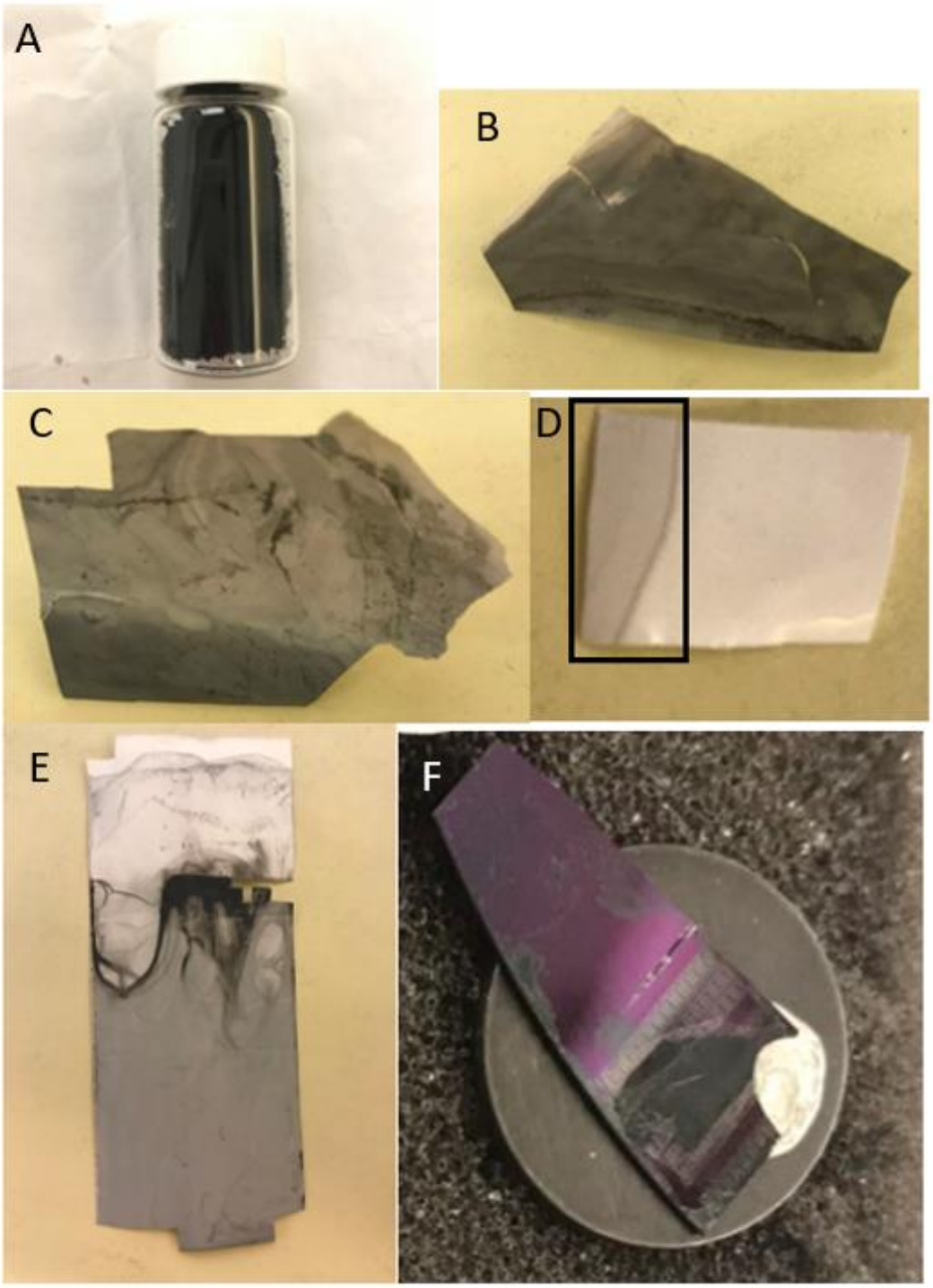

(Fig 5.5: A: CNT powder; B: dense random CNT film; C: less dense random CNT film; D: well-aligned CNT film; E: denser well-aligned CNT film F: Well-aligned CNT on Si substrate with gold electrodes)

Samples in this experiment are produced by ATOM Inc. Carbon nanotubes here are synthesized by CVD. It is said that well aligned sample are made through water-based solution and non-well aligned samples are made by depositing CNT solution on the film. The substrates of sample B-E are polymer and substrate of sample F is Si with gold electrodes. Sample B-D are said to be randomly aligned sample while sample D-F are said to have aligned CNTs.

6. Results and discussion

6.1 Raman Spectroscopy and Raman Imaging

In this research, both Raman Spectroscopy and Raman Imaging are used to probe the diameter of CNT, whether the sample contains metallic CNT, and whether there are defects on the sample.

Raman Spectroscopy was first done on CNT powder, dense Random CNT film, less dense CNT film and well-aligned CNT film. Since the strong RBM peaks only occur for metallic CNT, it is clear that metallic CNTs exist in CNT powder, dense random CNT film and less dense CNT film, while less or no metallic CNT exist in the well-aligned CNT film. It can also be seen from the RBM mode that only CNTs in well-aligned CNT film have the same diameter because there is only one RBM peak in this film. Since the peak position of RBM mode is $248/R_t\ cm^{-1}$, and the RBM peak of the well-aligned sample is 163 cm^{-1}, the diameter of CNTs in these samples is around 1.5nm. This can also be verified from the position of the G' band at 1580 cm^{-1}, which has a relation of $G^- = 1591 - (45.7,79.5)/d_t\ cm^{-1}$. According to [12] the bandgap of the carbon nanotubes is around 0.9eV.

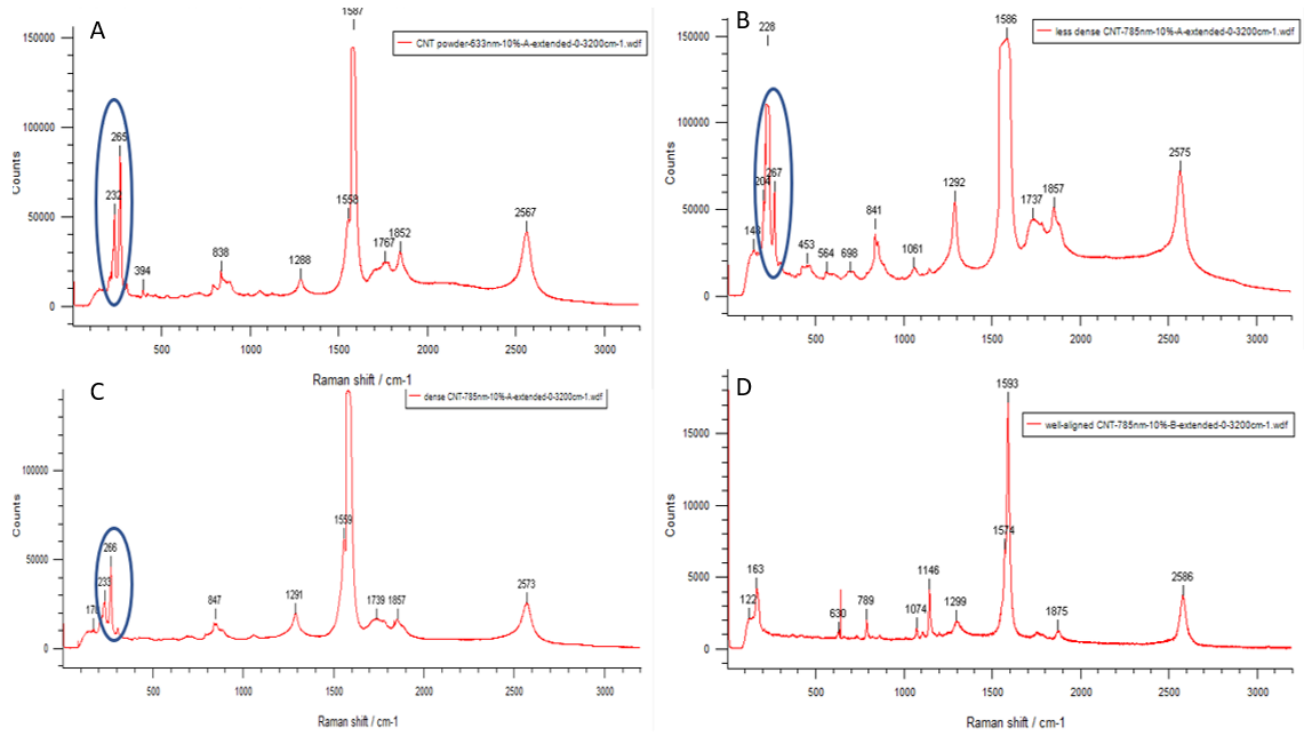

(Fig 6.1: Raman Spectra of (A): CNT powder;(B): Dense random CNT film;(C): Less dense CNT film;(D): Well-aligned CNT film)

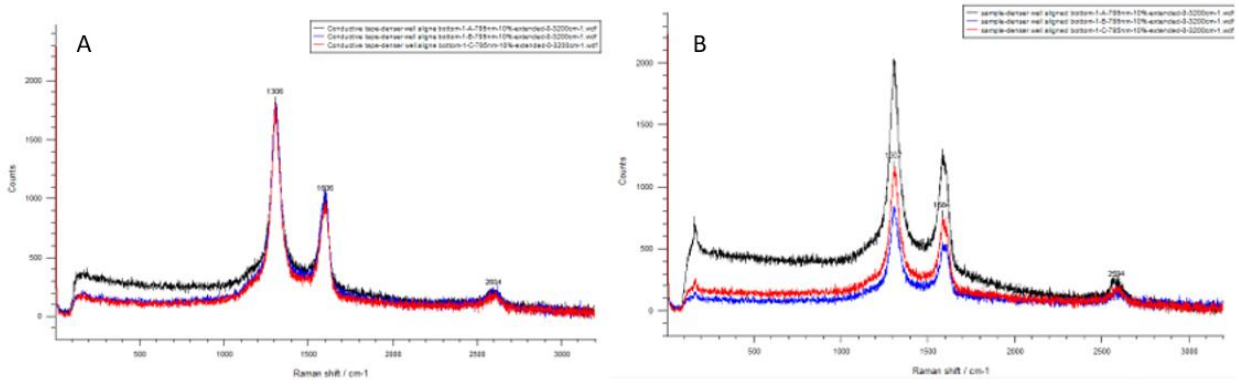

（Fig 6.2: (A) Raman Spectra of conductive tape (B):conductive tape with CNT on）

Raman spectroscopy can also be used to detect whether CNT exist or not. Fig 6.2 demonstrates an example of detecting the existence of carbon nanotubes on conductive tape, which contains carbon. As is shown in Fig 6.2 (A), there is only G band in this figure and no RBM peak can be seen. However, in Fig 6.2 (B), RBM peak appears when carbon nanotubes

are stick onto the conductive tape. Therefore, Raman spectroscopy can be a good way of detecting the existence of carbon nanotubes.

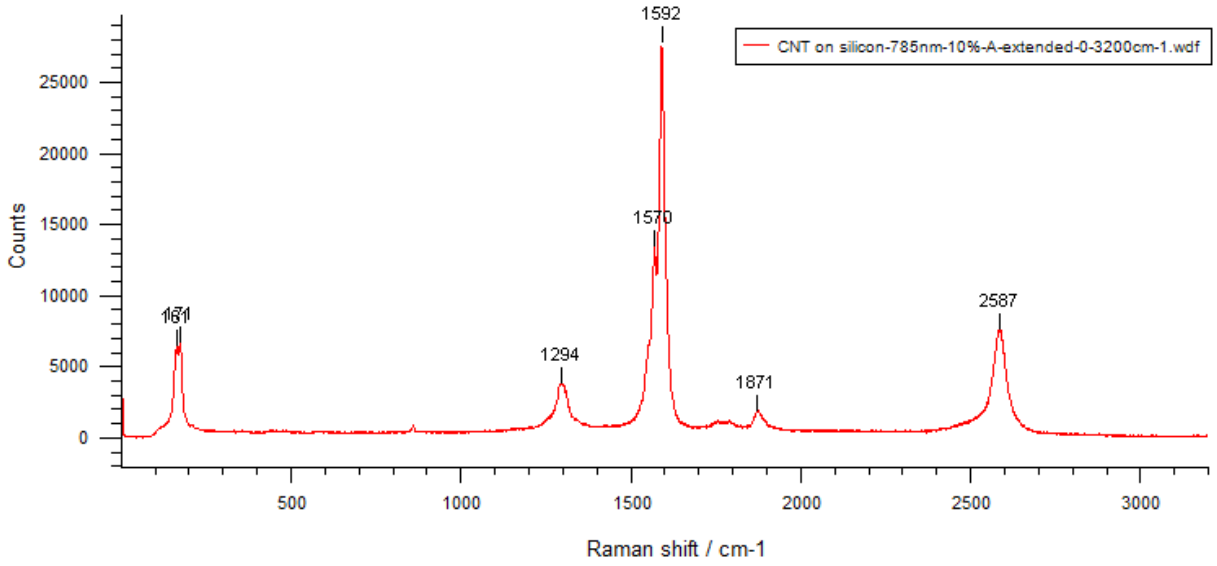

(Fig 6.3: Raman Spectra of CNT on Silicon wafer)

Raman spectra is also found to be quite surface-sensitive. Fig 6.3 is the Raman Spectra of CNT deposited on Si substrate. The thickness of CNT is measured through AFM to be 100-150nm. As is seen in Fig 6.3, the Raman peak of silicon at 520cm^{-1} is not significant.

Defect detection on the carbon nanotube film

Raman spectroscopy is first used to characterize defect on the surface, but no good result is obtained. As is seen in Fig 6.4, there is no significant difference in Raman Spectra between areas with defect and areas without defect.

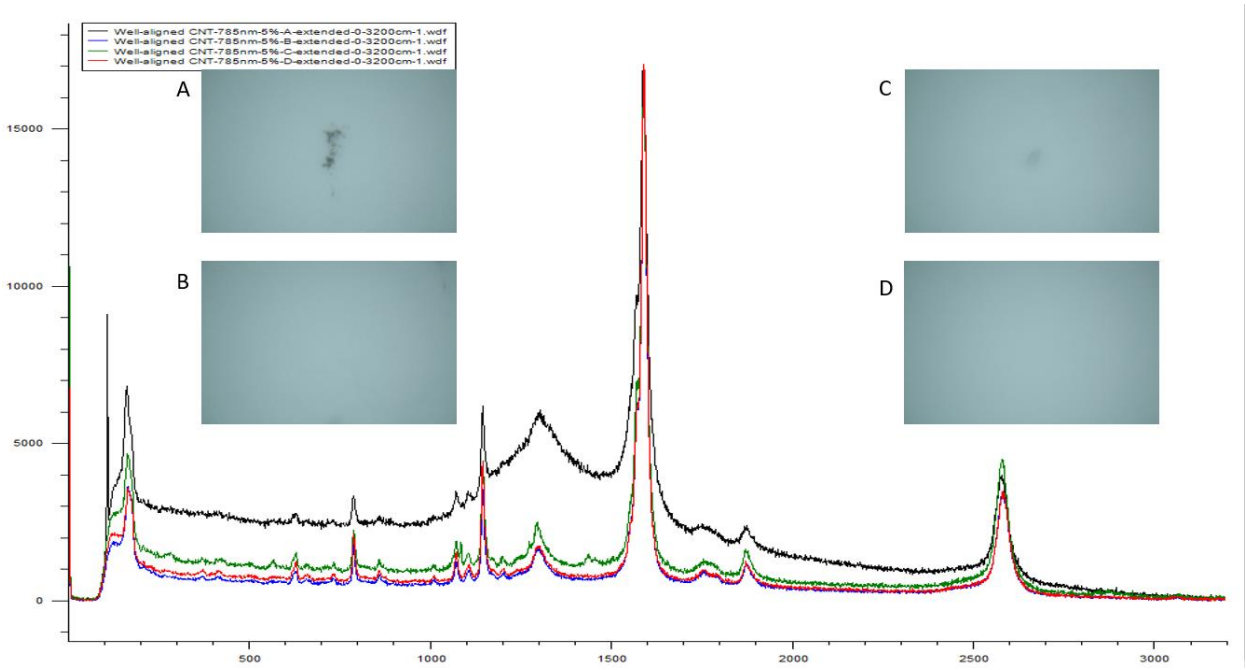

(Fig 6.4: Raman spectroscopy on CNT film with defects in photo image but no change in Raman Spectroscopy)

However, Raman Imaging proves to be a good way for defect detection. Two examples are demonstrated here. Fig 6.5 images the defect produced during deposition, which is probably an aggregation of carbon nanotubes. It can be clearly seen that the G band intensity at the dark spots are higher, while the intensity at its boundary is lower. There is no significant difference between the spectra of these two spots, so these dark spots are probably aggregation of carbon nanotubes.

Fig 6.6 images the defect created during SEM imaging. The Raman spectra of the darker area in the optical image, which is probably CNT burnt during exposure of electron beam, is significantly different from that of unburnt areas. A good resemble of Raman image is obtained by choosing only the edge of G band for imaging, and the Raman Image pattern resembles that of the optical image.

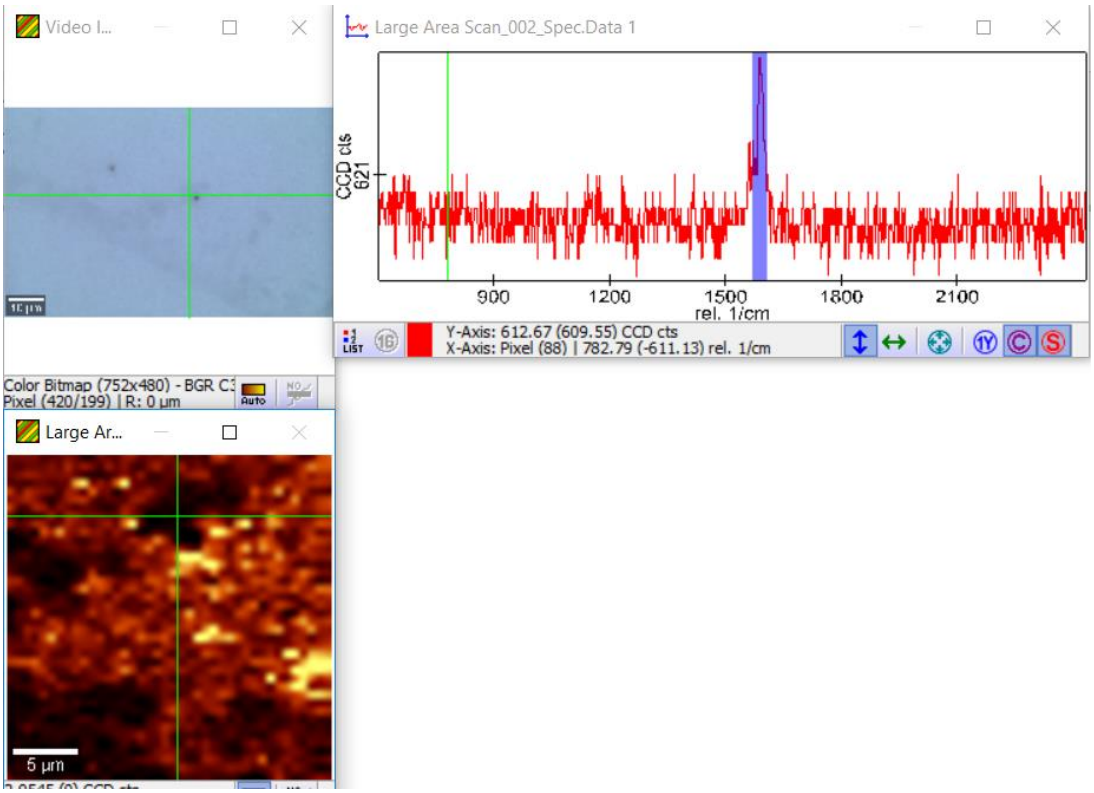

(Fig 6.5: Raman microscopy on defects on CNT film)

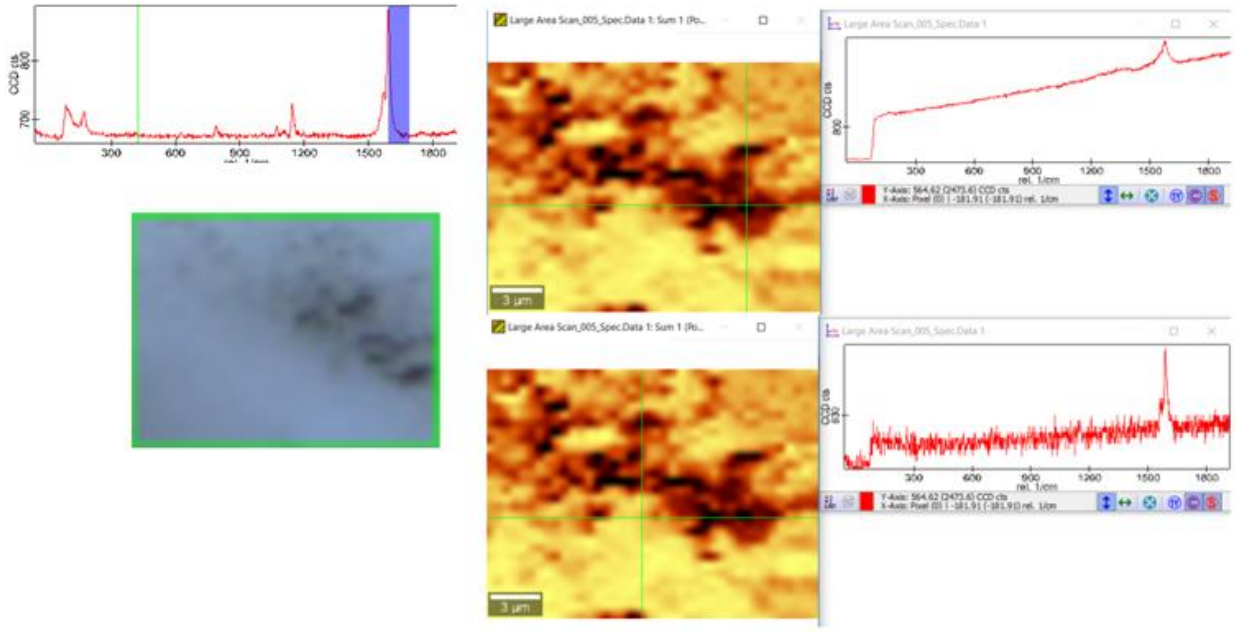

(Fig 6.6: Raman Imaging on Well-aligned CNT film burnt by electron beam)

Damage during measurement

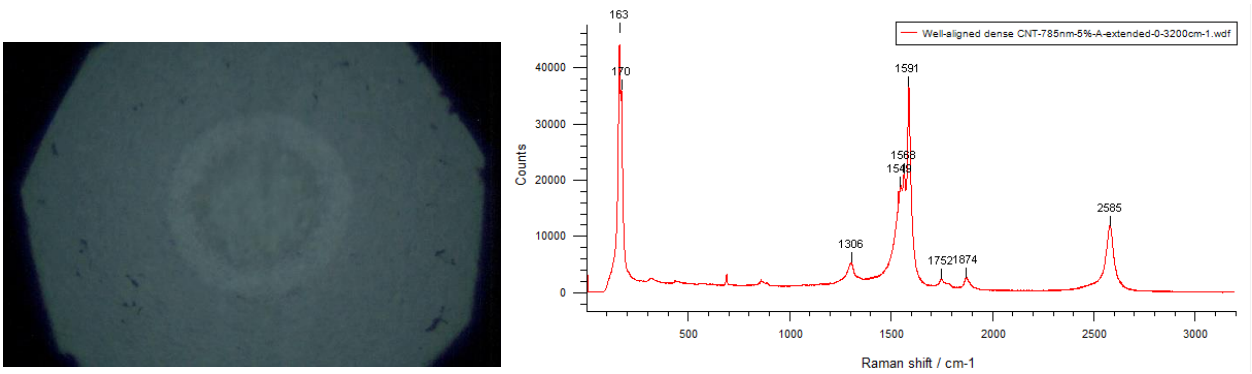

(Fig 6.7: Overheating of sample containing metallic CNT)

Raman spectroscopy is in most cases a non-destructive technique, however, laser could cause damage to the sample under certain circumstances. If the power of the laser is too high, it could cause damage of the sample. It was observed during experiment that laser beam would cause damage to the sample when the laser power is 10mW. Samples containing metallic carbon nanotubes are also found to be overheated during the test. As is seen in Fig 6.7, the optical image of the area under the laser spot was changed after performing Raman spectroscopy. All the samples that was observed to be overheated contain metallic carbon nanotubes, while all samples with only semiconducting carbon nanotubes shows no burning no matter how thick the carbon nanotube layer is. For the burnt sample, no change is detected in the Raman Spectra. Therefore, we can conclude that the overheating of the sample results from the existence of metallic carbon nanotubes, and Raman spectroscopy will not cause damage to the sample. However, since the Raman spectra do not change before and after the burnt after several measurements on the same spot, it can be concluded that the heat generated is probably not enough to burn the carbon nanotubes.

6.2 SEM imaging

In order to test SEM's ability of imaging CNT, we first tried to image the carbon nanotube powder stick onto the conductive tape. Good SEM image was obtained at 1kV. CNT bundles can be seen in this sample and the resolution can go down to around 10nm. Charging effect is not observed in this sample.

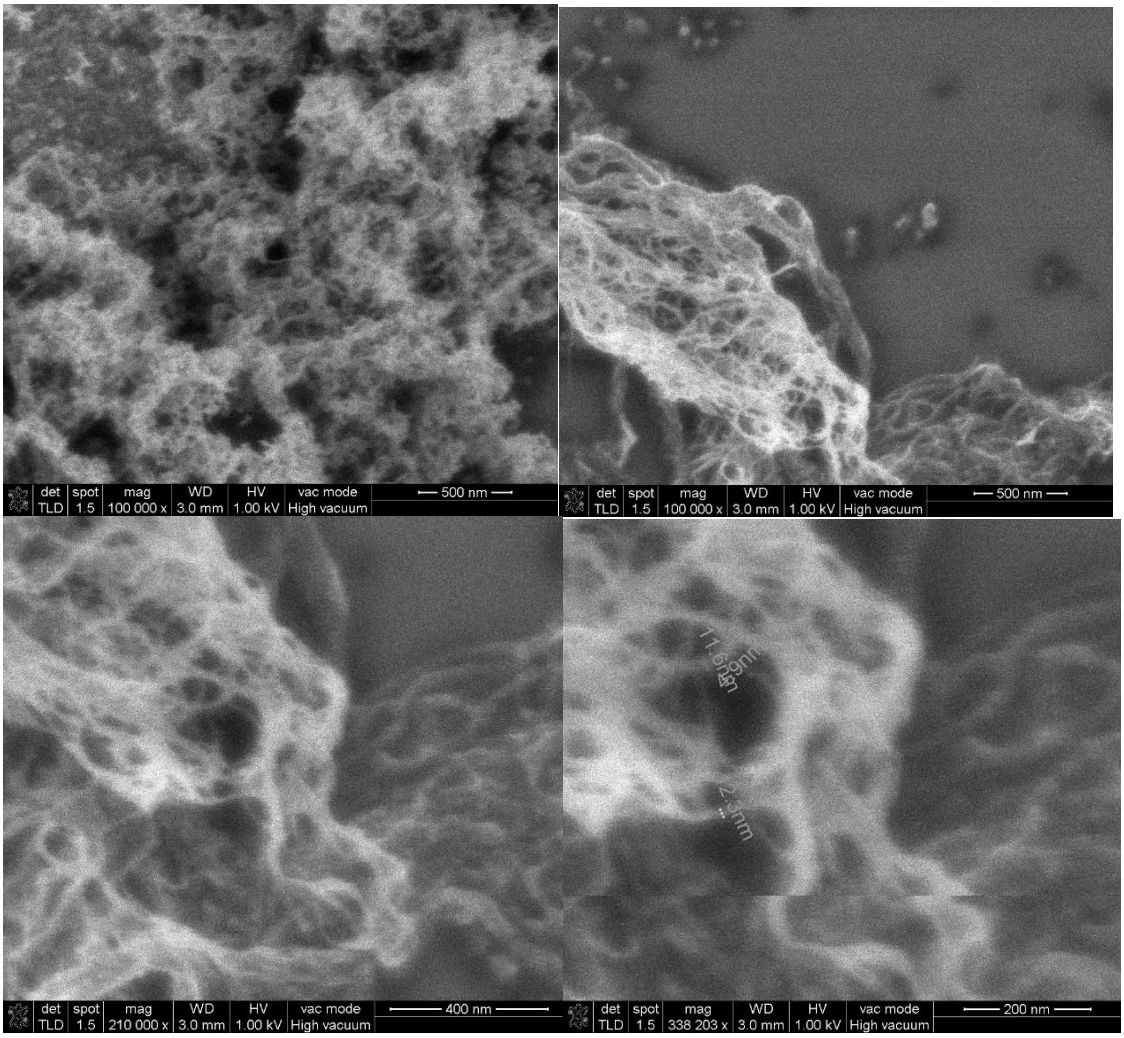

(Fig 6.8: SEM image of CNT powder)

However, it becomes very difficult to achieve a resolution of 1.5nm when carbon nanotubes are deposited onto substrates. The first obstacle is conductivity. SEM imaging was first performed on less dense well-aligned sample, but charging was very severe and the

sample was burnt. As is shown in Fig 6.9, etching happened at the edge of the sample after performing SEM imaging. This sample was also characterized by Raman imaging before gold deposition, as is stated in the last session. Denser well-aligned sample was also used but charging was still severe for them. Therefore, multiple methods were used for diminishing charging effect.

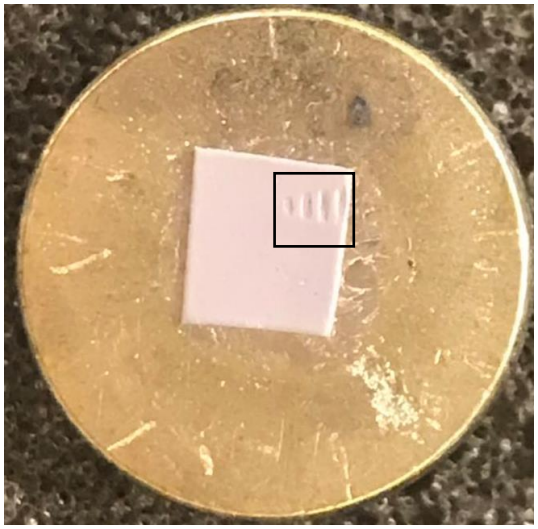

(Fig 6.9: Well-aligned CNT sample burnt during SEM imaging)

The first way is depositing gold on the sample. This is a typical way of reducing electron accumulation on the SEM sample. However, it is not sure whether gold deposition will cover up the small features on the sample since the diameter of the carbon nanotubes is 1.5nm, so the deposition of gold was performed on CNT powder. As is shown in Fig 6.10, although gold deposition greatly enhanced conductivity, small features such as the spacing between aggregated carbon nanotubes were buried under the gold layer. Gold deposition for this sample only took 30s, which is the minimum time to form a continuous layer of gold. A shorter deposition time may lead to gold island on the surface of the sample, which may cause a failure in reducing charging. Therefore, depositing gold is not a suitable way to enhance the conductivity of the sample.

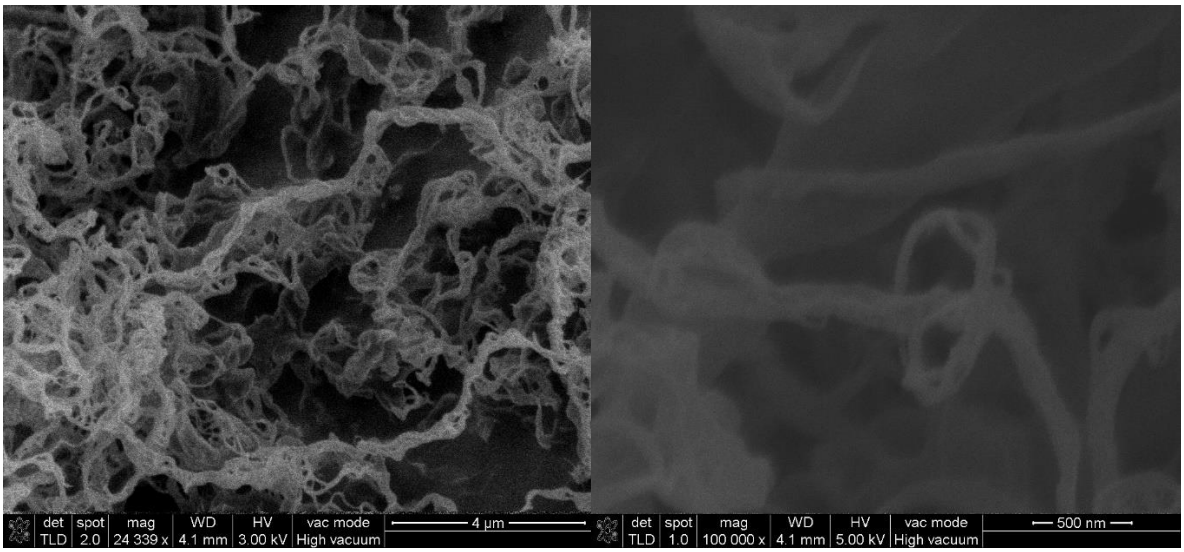

(Fig 6.10: Carbon nanotube powder with gold deposition for 30s)

The second method is applying conductive paint on the edge of the sample. There are two reasons for performing this step. First, conductive paint has a higher conductivity than conductive tape. Second, the substrate of the sample is non-conductive polymer, and there exist no channel for the charge on the surface of the sample to be conducted to ground. Therefore, conductive paint is applied on the edge of the sample. The sample is still connected to the stub by conductive tape since samples are easily pilled off when they are glued by conductive paint.

This method do enhanced the conductivity of the sample, but charging still exist. We can see that carbon nanotubes can be imaged at the edge of the sample, but images are blur on the surface of the sample. Also, since conductivity is still poor for this sample, damage still occurs. After performing SEM for a long time, the sections few µms away from the conductive paint started to be over heated, and small wrenches began to appear. The reason is probably that the CNTs of this sample do not have enough conductivity and is not long enough, so that the areas with no CNTs connected to the conductive paint was still not grounded. Meanwhile, the conductive paints, which uses silver particles to enhance conduction, oxidized during the time,

so the conductivity of the sample was observed to drop with time. To further reduce the charging effect and achieve permanent enhancement of conductivity, carbon nanotubes were deposited on Si substrate with gold electrodes.

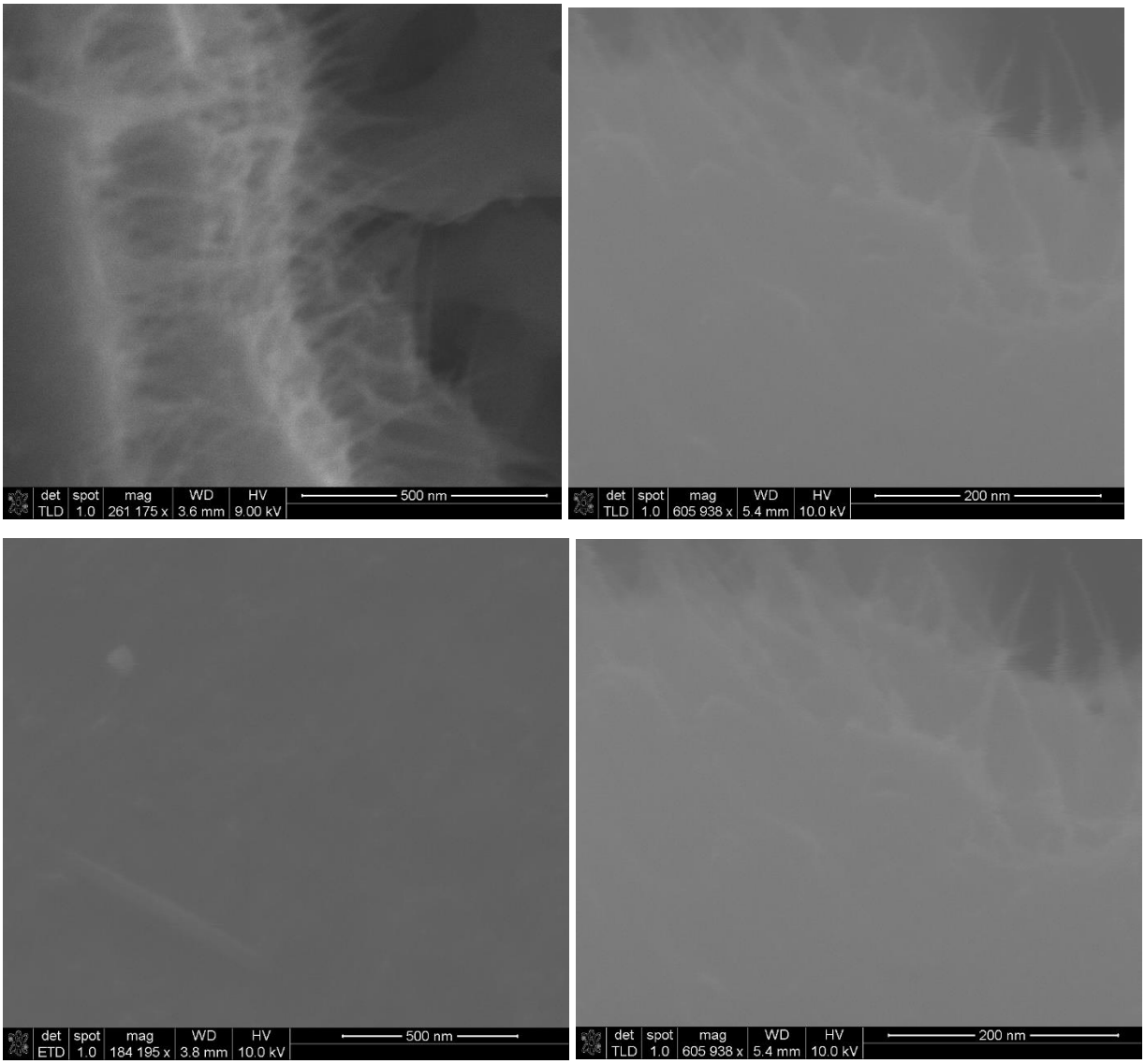

(Fig 6.11: SEM imagae at the edge of denser well aligned carbon nanotubes deposited polymer)

For carbon nanotubes deposited on Si substrate with gold electrodes, charging effect was mostly diminished and SEM images were easily obtained. The best accelerating voltage was found to be 8-10kV. These images clearly show that there are both well-aligned and mis-aligned carbon nanotubes on the surface, and there are unknown particles on the surface.

However, even the best picture failed to provide a satisfactory solution on aggregated carbon nanotubes. As is shown in Fig 6.12, even though good resolution can be obtained for carbon nanotubes that falls into a pit, carbon nanotubes on the substrate surface were still hard to tell. Also, since individual carbon nanotubes cannot be told apart, it is still unknown whether the broader lines are CNT bundles or not. Working distance of 3-5mm was also adjusted, but no higher resolution was obtained. As is seen in Fig 6.13, adjusting the working function did not lead to a significant improvement in the resolution of SEM image for this sample. At the same time, SEM was observed to damage the sample during imaging. CNTs were found to be burnt at 10kV under an exposure time of 700us. Since charging effect was almost diminished and the damage of sample was observed, SEM is probably not a good method for CNT deposited film imaging.

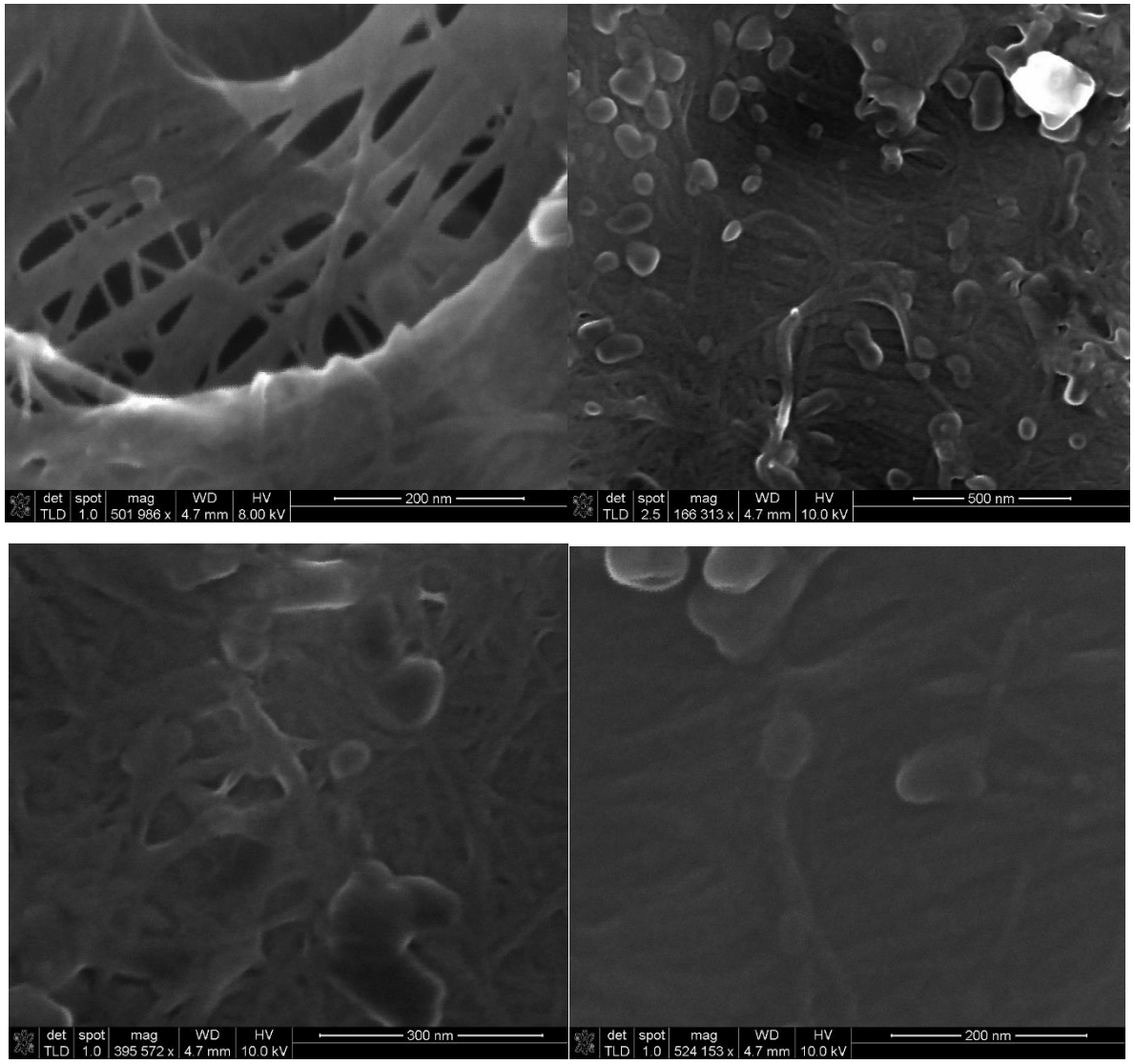

(Fig 6.12: SEM image of CNT deposited on Si substrate with gold electrodes)

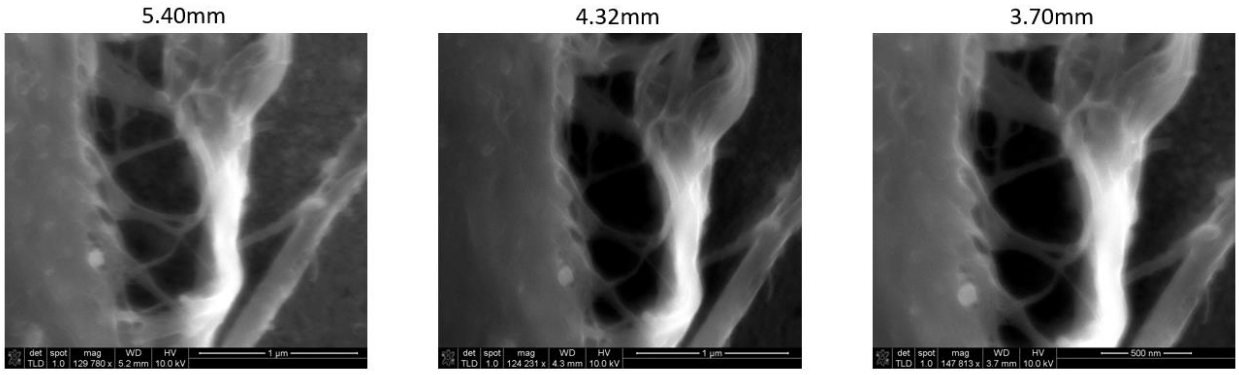

(Fig 6.13: SEM image under difference working distances)

6.3 AFM imaging

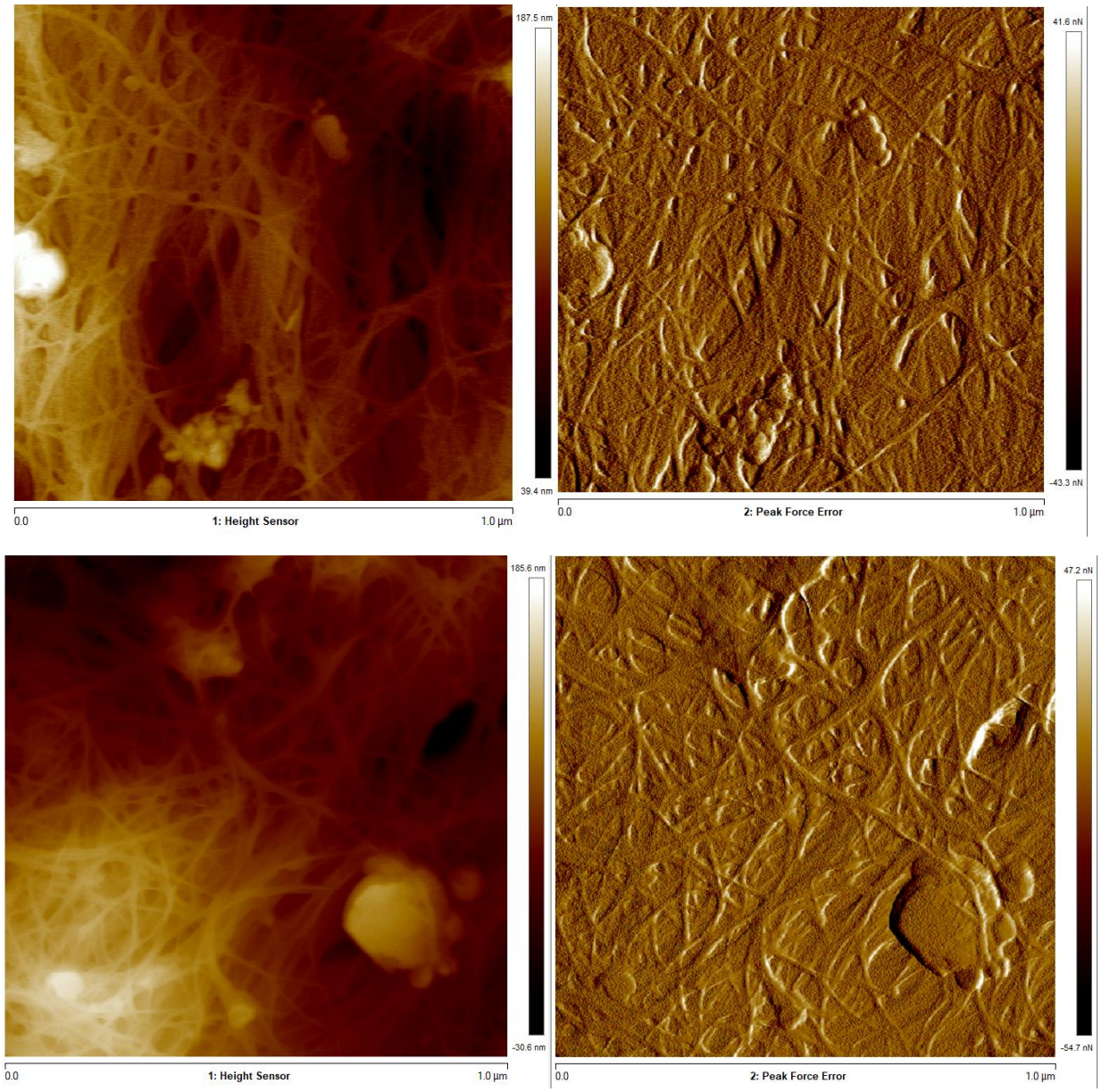

(Fig 6.14: AFM image on CNT deposited on Si substrate)

AFM imaging proved to be a non-destructive method for imaging deposited carbon nanotubes with a resolution good enough to tell apart individual carbon nanotubes. Experiments were done at CNT deposited on Si wafer, and images were obtained through ScanAnlysis mode. The minimum diameter of the nanotubes measured by AFM is around 2nm, which is

comparable to the diameter of the carbon nanotubes measured through Raman. Therefore, the resolution of AFM is good enough for imaging single walled carbon nanotubes. Scanning has been done on the same area for several times and no change in morphology is observed, thus AFM will not cause a damage to the sample. In these AFM images, it can be seen that both random and well-aligned CNT exist in the sample, and there exist unknown particles. This is identical with the results obtained in SEM.

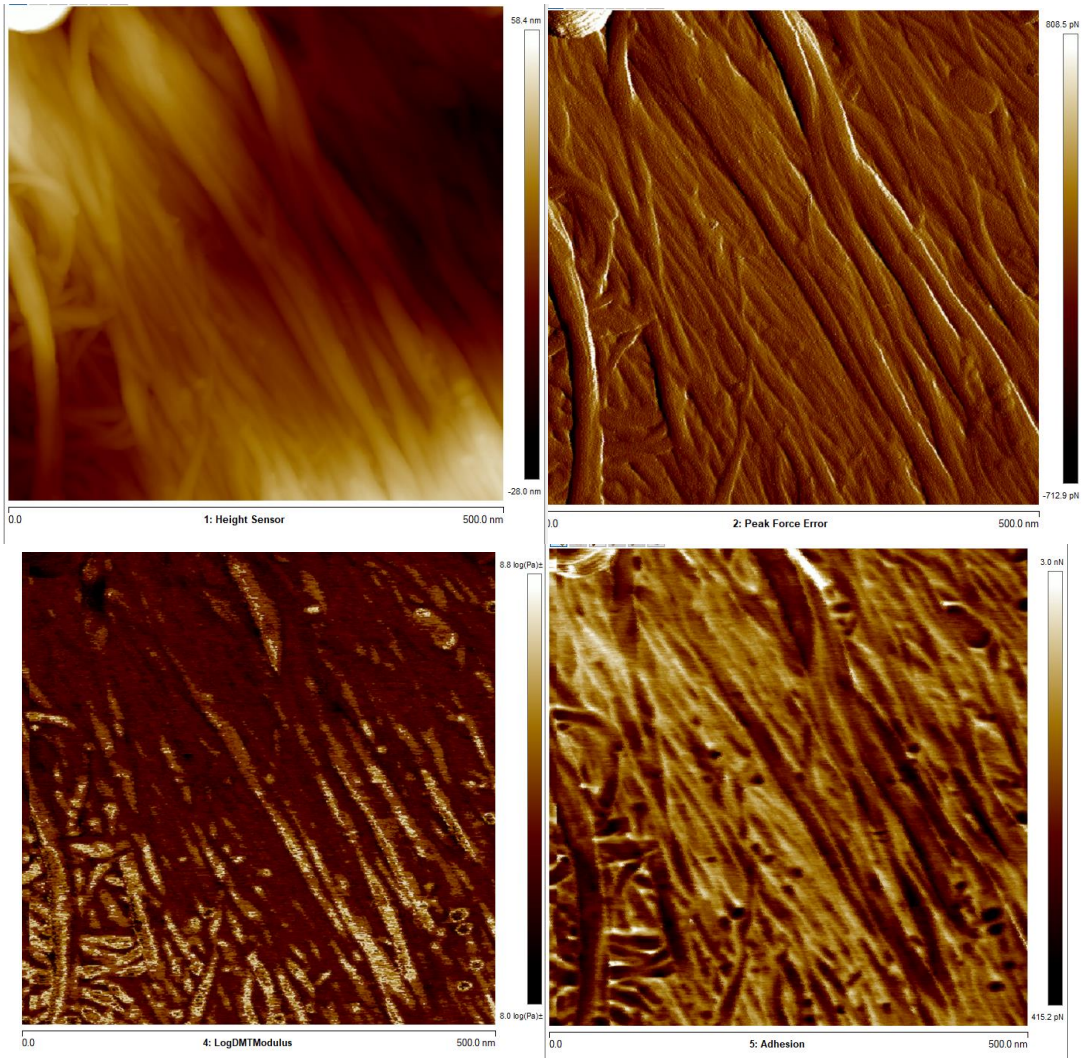

(Fig 6.15: A: Height image; B: Peak Force error; C: LogDMT Modulus D: Adhesion)

However, the height imaging through AFM sometimes failed to tell apart individual carbon nanotubes when they are aggregated. Therefore, mechanical AFM is also applied to

obtain more information. From the mechanical AFM images, it can be seen that individual carbon nanotubes can be told apart in adhesion imaging. The thicker bundles observed in SEM are carbon nanotubes bundles.

Electrostatic AFM

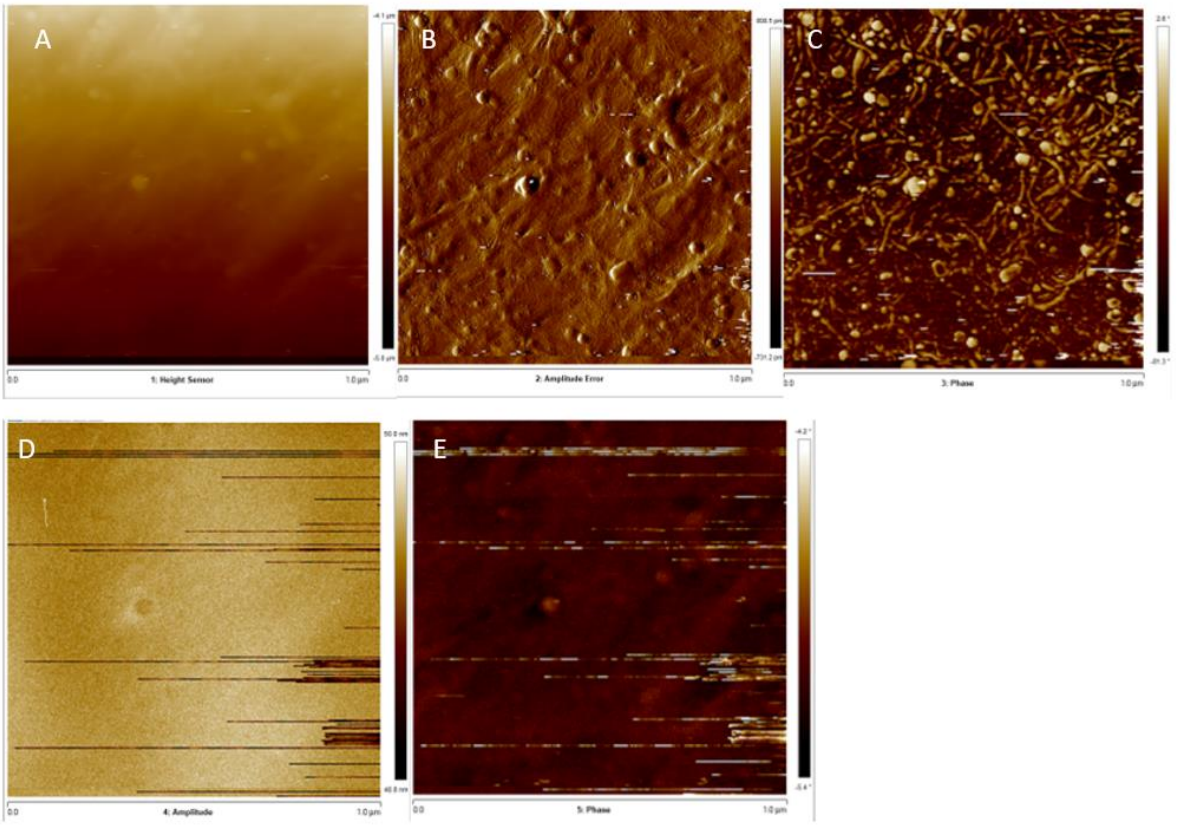

(Fig 6.16:Elelctrostatic AFM image of carbon nanotubes deposited on Si substrate:(A) Height image;(B): Amplitude image of surface morphology; (C): Phase image of surface morphology;(D) Amplitude image of AFM tip; (E): Phase image of AFM tip)

Electrostatic AFM was also applied to see the variation of surface potential on the sample. As is shown in Fig 6.16 (A)-(C) are typical surface morphology images, while (D)-(E) are electrostatic images. It can be observed that surface potential difference exists for carbon nanotubes and the impurities on the surface, as is shown in the surface morphology images. The success of electrostatic image indicate that further electrical measurements could be done through AFM.

7. Conclusion and future work

7.1 Conclusion

In conclusion, this thesis demonstrates that a combination of theoretical simulation and experimental characterization could be performed. In simulation part, it has been demonstrated that I-V curve can be plot through finite element method simulation and the effect of alignment defect can be simulated to direct how the characterization experiment should be designed. It has been shown that Raman Spectra is a good way for characterizing the diameter of carbon nanotubes and the composition of it. At the same time, Raman imaging is a good way for detecting damage and aggregation. As regards to imaging of the sample, AFM proves to be a good way for imaging the morphology of deposited carbon nanotubes in a non-destructive way, and the resolution can go down to 1.5nm. It has also been shown that mechanical properties and electrical properties can also be obtained for deposited carbon nanotubes through AFM. This may provide a way for characterizing the effect of defects on the performance of electronic devices.

7.2 Future work

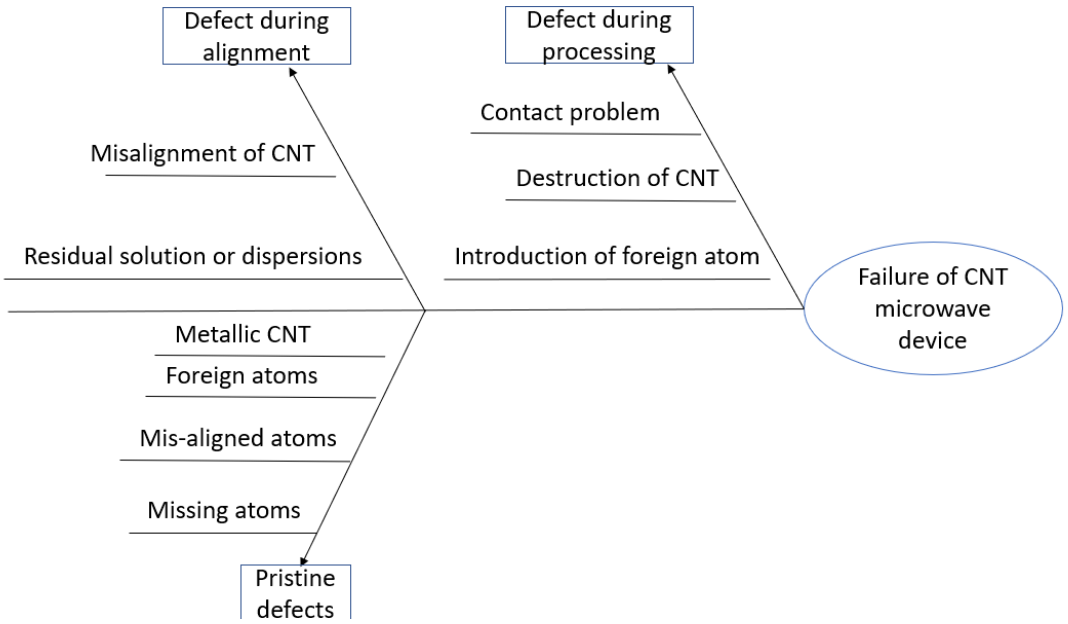

(Fig 7.1: Possible defects that would affect the performance of CNT electronic device)

Misalignment is not the only defect that could degradate the performance of carbon nanotubes FETs. As is shown in Fig 7.1, many other defects could also affect the performance of them. Further work should be done on characterizing the effect of other defects.

More works should also be done on the simulation part. First, this model is set up by assuming the carbon nanotubes resembles semiconductor equilibrium, so it is only suitable for solving the DC state, and other models should be used for the AC performance. Also, properties like the capacitance of CNT junction is not considered in this case. Other simulation methods that are more suitable for smaller dimensions should also be applied for the simulation of CNT junctions. Also, the nanotubes are set to be solid and cubic in this thesis, while real carbon nanotubes are actually hollow and round. Therefore, the deplesion behavior would be different and the degredation of electric field can only happen along the tube. At the same time, since carbon nanotubes are round, the contacting area between two different carbon nanotubes also requires consideration.

The capacitance of CNT junction may also be obtained through experimental characterization. Capacitance AFM may be a good choice. Though previous researches have been done through conductive AFM on CNT junction and bundles, they do not measure the AC properties of CNT, so they are not that useful for characterizing high frequency performance of CNT. Furthermore, they are done on carbon nanotubes with different diameters, which could be difficult to tell how much misalignments affects the electrical properties. However, sampling may be a potential problem to obtain good results. The performance of capacitance AFM requires a high conductivity for every connecting part outside the sample. For a complex network of carbon nanotubes, the behavior of individual junction would be hard to characterize since evey junction is connected. It may be a good way to use well-aligned carbon nanotubes sample with occational mis-aligned carbon nanotubes. Besides, the capacitance of CNT junction could be affected by many properties like the distance between the CNT and the residual solution as well. Resolution may also limit the performance of conductive AFM. Sharper conducting tip such as doped semconductor tip should be used.

A combination of traditional electronic device measurement, such as C-V curve measurement, with AFM could also be a way to achieve better characterization of defects. However, this requires characterizing the metal-contact of CNT devices first, which is still a challenge. The fabrication of reliable contact could also be a challenge since CNTs are ultra small in dimension.

For characterization of defects on the CNT sample, Tip-enhanced Raman Spectroscopy(TERS) may also be a better choice for detecting the compositional change in CNT film. Compared with Raman microscopy, TERS gives both the morphology and Raman signal of the surface. Also, the resolution of TERS can go down to a few nanometer, while the resolution of Raman Microscopy can only achieve around 200nm due to Rayleigh’s effect.

Appendix

1. Convergence plot for simulation for I-Vd curve of well-aligned nanotube FET

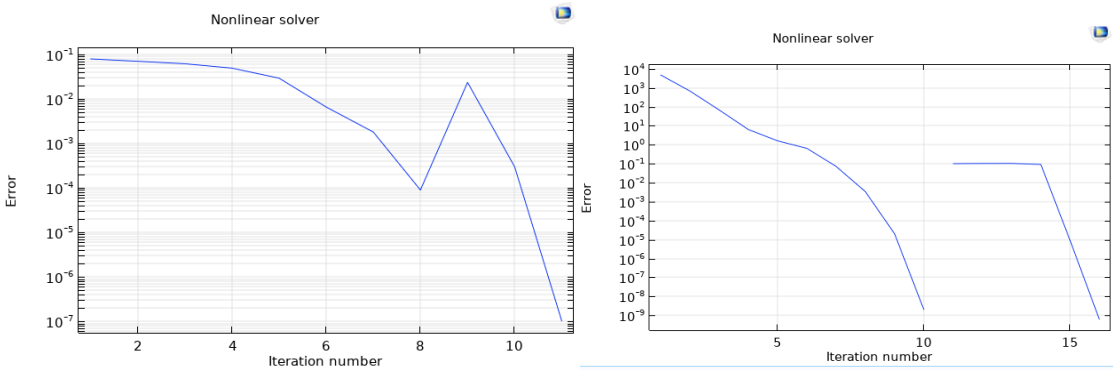

2. Three times simulation results of performing FEM simulation on well-aligned nanotube FET with crossing nanotube on top and their convergence plots

   Electron distribution

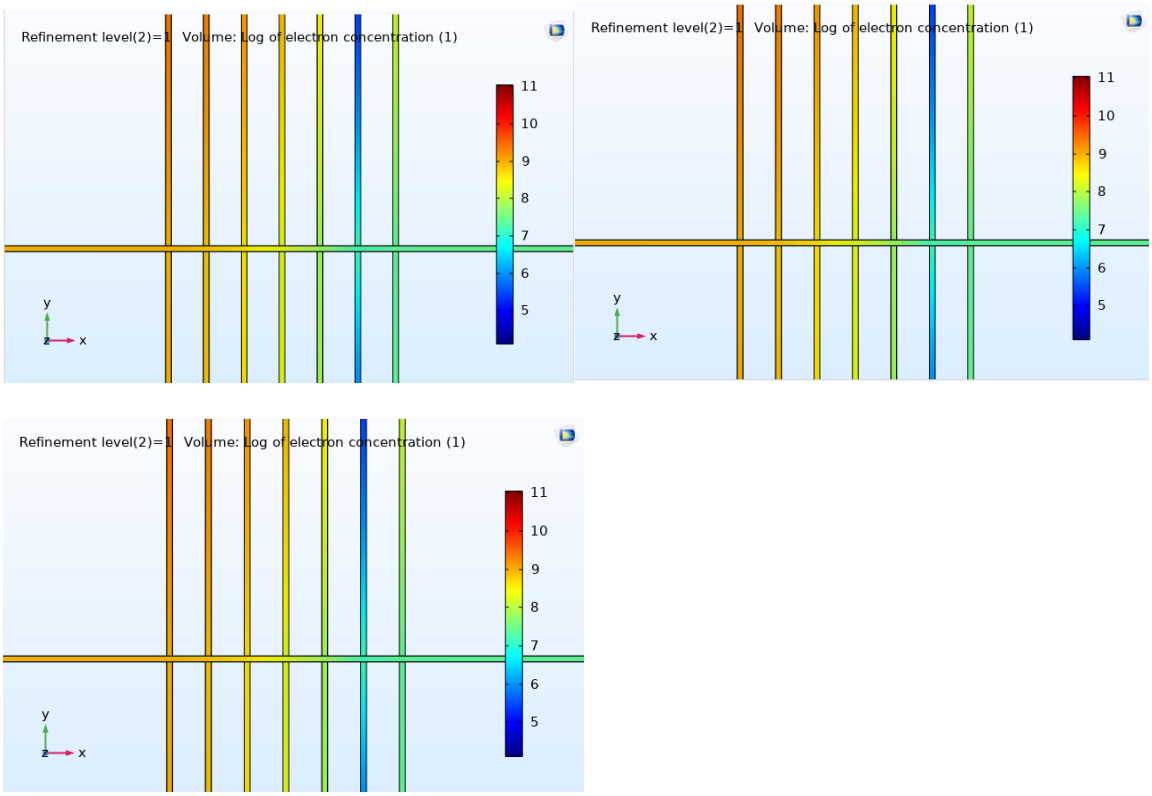

Hole distribution

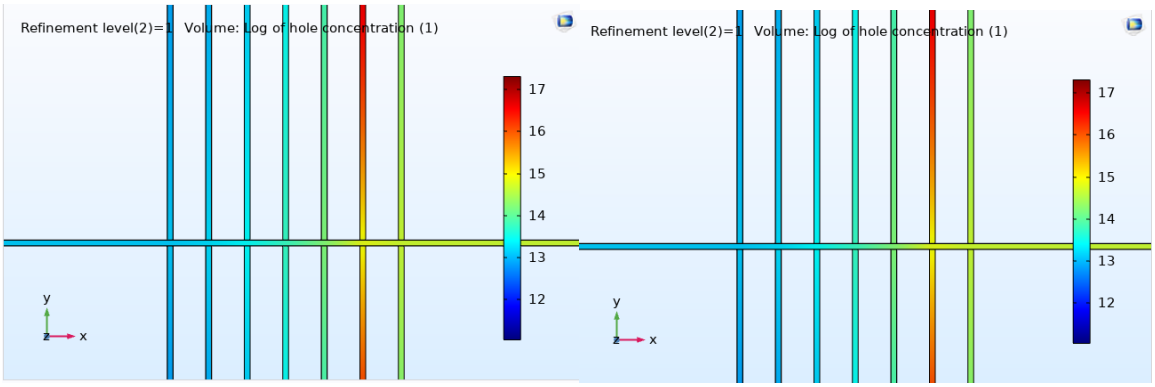

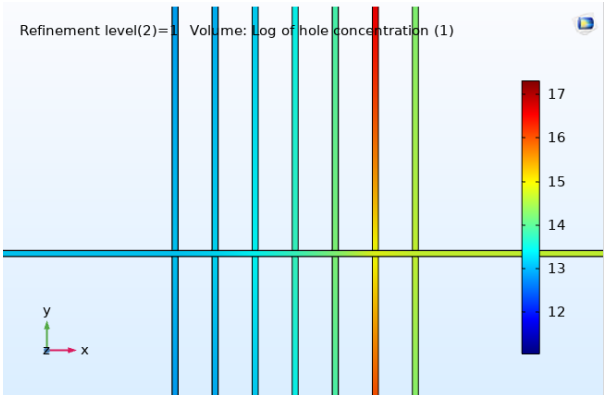

Electric field distribution

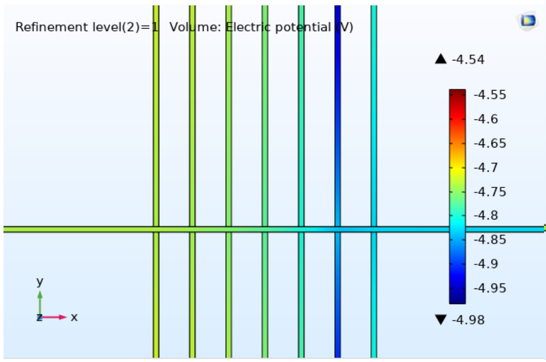

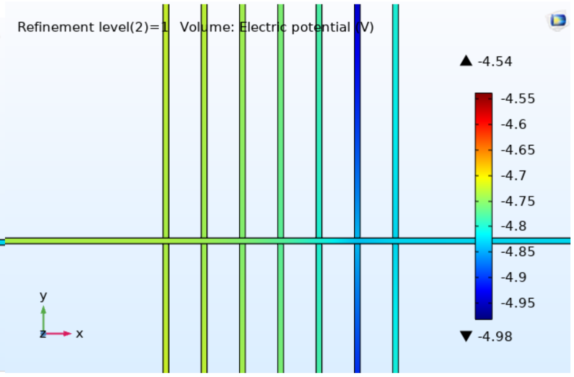

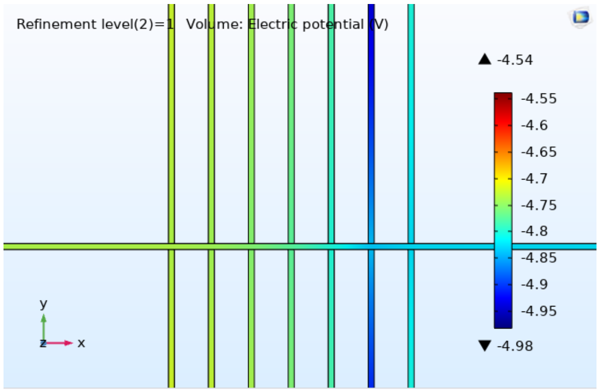

Convergence Plots

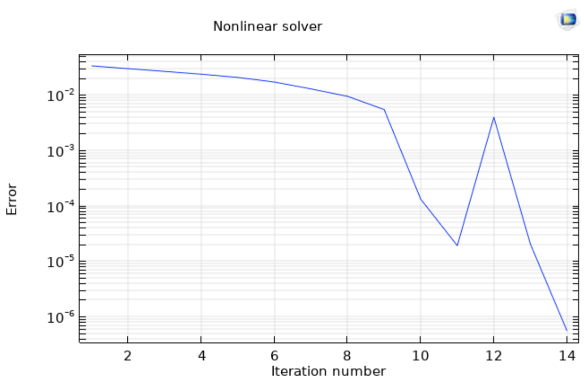

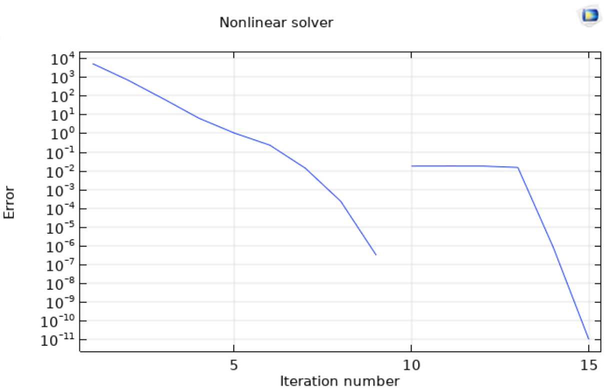

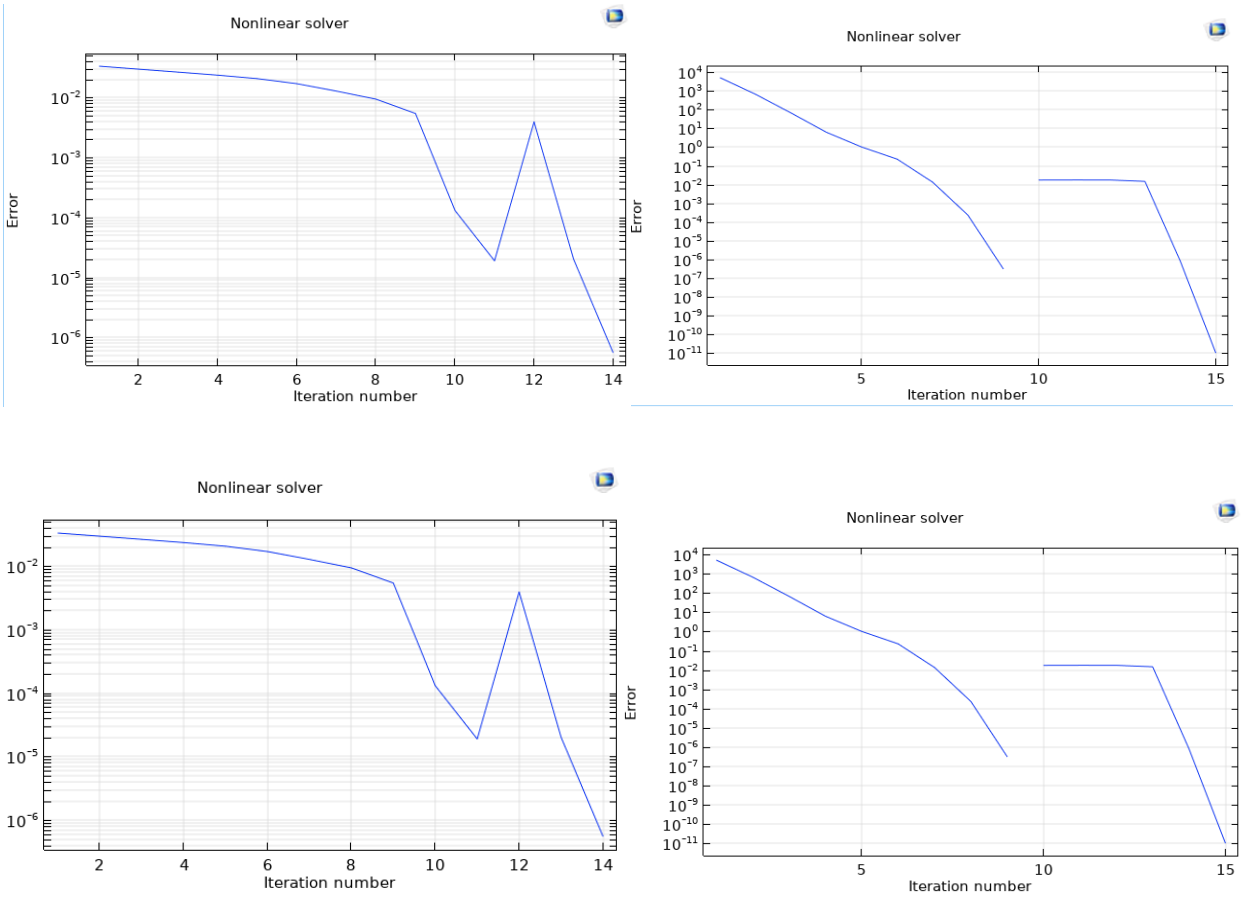

3. Convergence Plot for I-Vg curve for well-aligned nanotube FET with crossing nanotube on top

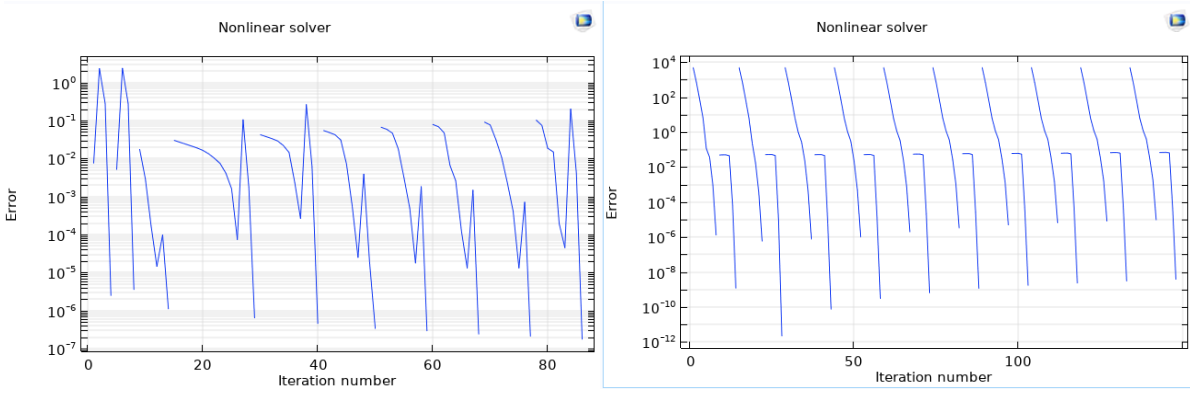

4. Convergence Plot for I-Vd curve for well-aligned nanotube FET with crossing nanotube on top

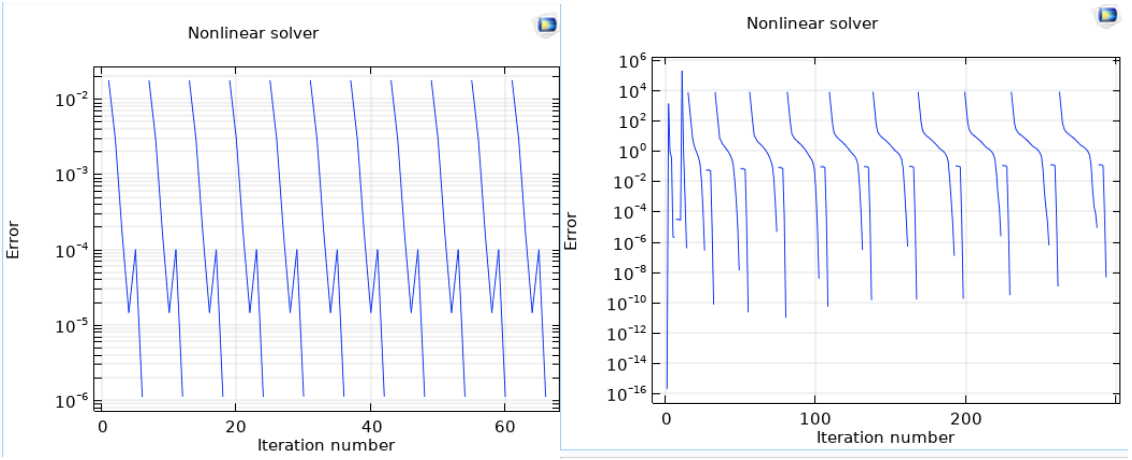

Reference

[1] Iijima, Sumio. "Helical microtubules of graphitic carbon." *nature* 354.6348 (1991): 56.

[2] Yu, Min-Feng, et al. "Strength and breaking mechanism of multiwalled carbon nanotubes under tensile load." *Science*287.5453 (2000): 637-640.

[3] Schadler, L. S., SC and Giannaris, and P. M. Ajayan. "Load transfer in carbon nanotube epoxy composites." *Applied physics letters* 73.26 (1998): 3842-3844.

[4] Tans, Sander J., Alwin RM Verschueren, and Cees Dekker. "Room-temperature transistor based on a single carbon nanotube." *Nature* 393.6680 (1998): 49.

[5] McEuen, Paul L., Michael S. Fuhrer, and Hongkun Park. "Single-walled carbon nanotube electronics." *IEEE transactions on nanotechnology* 99.1 (2002): 78-85.

[6] Martel, Richard, et al. "Single-and multi-wall carbon nanotube field-effect transistors." *Applied physics letters* 73.17 (1998): 2447-2449.

[7] Mawhinney, Douglas B., et al. "Infrared spectral evidence for the etching of carbon nanotubes: ozone oxidation at 298 K." *Journal of the American Chemical Society* 122.10 (2000): 2383-2384.

[8] Cheung, William, et al. "DNA and carbon nanotubes as medicine." *Advanced drug delivery reviews* 62.6 (2010): 633-649.

[9] Wilder, Jeroen WG, et al. "Electronic structure of atomically resolved carbon nanotubes." *Nature* 391.6662 (1998): 59.

[10] Khan, Waseem, Rahul Sharma, and Parveen Saini. "Carbon nanotube-based polymer composites: synthesis, properties and applications." *Carbon Nanotubes-Current Progress of their Polymer Composites*. IntechOpen, 2016.

[11] Jorio, Ado, Gene Dresselhaus, and Mildred S. Dresselhaus, eds. *Carbon nanotubes: advanced topics in the synthesis, structure, properties and applications*. Vol. 111. Springer Science & Business Media, 2007.

[12] Jorio, A., et al. "Structural (n, m) determination of isolated single-wall carbon nanotubes by resonant Raman scattering." *Physical Review Letters* 86.6 (2001): 1118.

[13] Odom, Teri Wang, et al. "Atomic structure and electronic properties of single-walled carbon nanotubes." *Nature*391.6662 (1998): 62.

[14] Cassell, Alan M., et al. "Large scale CVD synthesis of single-walled carbon nanotubes." *The Journal of Physical Chemistry B* 103.31 (1999): 6484-6492.

[15] Kong, Jing, Alan M. Cassell, and Hongjie Dai. "Chemical vapor deposition of methane for single-walled carbon nanotubes." *Chemical Physics Letters* 292.4-6 (1998): 567-574.

[16] Hafner, Jason H., Chin Li Cheung, and Charles M. Lieber. "Direct growth of single-walled carbon nanotube scanning probe microscopy tips." *Journal of the American Chemical Society* 121.41 (1999): 9750-9751.

[17] Nikolaev, Pavel, et al. "Gas-phase catalytic growth of single-walled carbon nanotubes from carbon monoxide." *Chemical physics letters* 313.1-2 (1999): 91-97.

[18] Kokai, F., et al. "Growth dynamics of single-wall carbon nanotubes synthesized by CO2 laser vaporization." *The Journal of Physical Chemistry B* 103.21 (1999): 4346-4351.

[19] Dupuis, Anne-Claire. "The catalyst in the CCVD of carbon nanotubes—a review." *Progress in materials science* 50.8 (2005): 929-961.

[20] Liao, Yongping, et al. "Direct Synthesis of Colorful Single-Walled Carbon Nanotube Thin Films." *Journal of the American Chemical Society* 140.31 (2018): 9797-9800.

[21] Ding, Lei, et al. "Selective growth of well-aligned semiconducting single-walled carbon nanotubes." *Nano letters*9.2 (2009): 800-805.

[22] Krupke, Ralph, et al. "Separation of metallic from semiconducting single-walled carbon nanotubes." *Science*301.5631 (2003): 344-347.

[23] Li, Jingqi, et al. "Fabrication of carbon nanotube field effect transistors by AC dielectrophoresis method." *Carbon* 42.11 (2004): 2263-2267.

[24] Javey, Ali, et al. "Ballistic carbon nanotube field-effect transistors." *nature* 424.6949 (2003): 654.

[25] Liu, Huaping, et al. "Large-scale single-chirality separation of single-wall carbon nanotubes by simple gel chromatography." *Nature communications* 2 (2011): 309.

[26] White, Carter T., and Tchavdar N. Todorov. "Carbon nanotubes as long ballistic conductors." *Nature* 393.6682 (1998): 240.

[27] Guo, Jing, Mark Lundstrom, and Supriyo Datta. "Performance projections for ballistic carbon nanotube field-effect transistors." *Applied Physics Letters* 80.17 (2002): 3192-3194.

[28] White, Carter T., and Tchavdar N. Todorov. "Carbon nanotubes as long ballistic conductors." Nature 393.6682 (1998): 240.

[29] Javey, Ali, et al. "High performance n-type carbon nanotube field-effect transistors with chemically doped contacts." *Nano letters* 5.2 (2005): 345-348.

[30] Sze, Simon M., and Kwok K. Ng. *Physics of semiconductor devices*. John wiley & sons, 2006.

[31] Fuhrer, M. S., et al. "Crossed nanotube junctions." *Science*288.5465 (2000): 494-497.

[32] Nirmalraj, Peter N., et al. "Electrical connectivity in single-walled carbon nanotube networks." *Nano letters* 9.11 (2009): 3890-3895.

[33] Zhang, Z. J., et al. "Substrate-site selective growth of aligned carbon nanotubes." Applied Physics Letters 77.23 (2000): 3764-3766.

[34] He, Xiaowei, et al. "Wafer-scale monodomain films of spontaneously aligned single-walled carbon nanotubes." *Nature nanotechnology* 11.7 (2016): 633.

[35] Park, Steve, et al. "Large-Area Assembly of Densely Aligned Single-Walled Carbon Nanotubes Using Solution Shearing and Their Application to Field-Effect Transistors." *Advanced Materials* 27.16 (2015): 2656-2662.

[36] LeMieux, Melburne C., et al. "Self-sorted, aligned nanotube networks for thin-film transistors." *Science* 321.5885 (2008): 101-104.

[37] Beyond CMOS. International Technology Roadmap for Semiconductors 2.0; 1-87; 2015.

[38] Chen, Yupeng. "Finite Element Method Modeling Of Advanced Electronic Devices." (2006).

[39] Bathe, Klaus-Jürgen. Finite element procedures. Klaus-Jurgen Bathe, 2006.

[40] COMSOL Multiphysics Reference Guide

[41] https://www.nanophoton.net/raman-spectroscopy/lessons/lesson-1

[42] Dresselhaus, Mildred S., et al. "Raman spectroscopy of carbon nanotubes." Physics reports 409.2 (2005): 47-99.

[43] Rao, A. M., et al. "Diameter-selective Raman scattering from vibrational modes in carbon nanotubes." Science 275.5297 (1997): 187-191.

[44] Dresselhaus, Mildred S., et al. "Perspectives on carbon nanotubes and graphene Raman spectroscopy." Nano letters10.3 (2010): 751-758.

[45] Fan, Yuwei, Brett R. Goldsmith, and Philip G. Collins. "Identifying and counting point defects in carbon nanotubes." *Nature materials* 4.12 (2005): 906.

[46] Osswald, Sebastian, et al. "Elimination of D-band in Raman spectra of double-wall carbon nanotubes by oxidation." *Chemical Physics Letters* 402.4-6 (2005): 422-427.

[47] Dillon, A. C., et al. "Systematic inclusion of defects in pure carbon single-wall nanotubes and their effect on the Raman D-band." *Chemical physics letters* 401.4-6 (2005): 522-528.

[48] https://www.witec.de/products/correlative-microscopes/rise/

[49] https://www.britannica.com/technology/scanning-electron-microscope

[50] Sergey.V.Prikhodko. Introduction to Materials Characterization: Electron Microscopy

[51] https://www.brukerafmprobes.com/p-3726-scanasyst-air.aspx

[52] https://www.brukerafmprobes.com/p-3950-scm-pit-v2.aspx